Int J Fract (2017) 208:145–170
https://doi.org/10.1007/s10704-017-0230-2

IUTAM BALTIMORE

A theoretical and computational framework for studying creep crack growth

Elsiddig Elmukashfi · Alan C. F. Cocks

Received: 12 March 2017 / Accepted: 29 June 2017 / Published online: 7 August 2017

Abstract In this study, crack growth under steady state creep conditions is analysed. A theoretical framework is introduced in which the constitutive behaviour of the bulk material is described by power-law creep. A new class of damage zone models is proposed to model the fracture process ahead of a crack tip, such that the constitutive relation is described by a traction-separation rate law. In particular, simple critical displacement, empirical Kachanov type damage and micromechanical based interface models are used. Using the path independency property of the C^*-integral and dimensional analysis, analytical models are developed for pure mode-I steady-state crack growth in a double cantilever beam specimen (DCB) subjected to constant pure bending moment. A computational framework is then implemented using the Finite Element method. The analytical models are calibrated against detailed Finite Element models. The theoretical framework gives the fundamental form of the model and only a single quantity $\hat{C}_k$ needs to be determined from the Finite Element analysis in terms of a dimensionless quantity ϕ_0, which is the ratio of geometric and material length scales. Further, the validity of the framework is examined by investigating the crack growth response in the limits of small and large ϕ_0, for which analytical expression can be obtained. We also demonstrate how parameters within the models can be obtained from creep deformation, creep rupture and crack growth experiments.

Keywords Creep · Crack · C*-integral · Damage zone model · Traction-separation rate law (TSRL) · Double cantilever beam (DCB) · Dimensionless analysis

E. Elmukashfi (✉) · A. C. F. Cocks
Department of Engineering Science, University of Oxford, Park Road, OX1 3PJ Oxford, UK
e-mail: elsiddig.elmukashfi@eng.ox.ac.uk

A. C. F. Cocks
e-mail: alan.cocks@eng.ox.ac.uk

Nomenclature

$2l$	The spacing between two adjacent pores
β	A material parameter of the exponential damage law
δ_n^{c}	The critical normal displacement jump in the damage zone at the crack tip
δ_n^{f}	The normal displacement jump at failure in the crack tip
δ_i	The displacement jump vector across the damage zone ($i = 1, 2, 3$)
$\dot{\delta}_0$	The separation rate at the reference traction T_0
$\dot{\delta}_n^{\mathrm{m}}$	The maximum normal displacement jump rate vector in the crack tip
$\dot{\delta}_i$	The displacement jump rate vector across the damage zone ($i = 1, 2, 3$)
$\dot{\varepsilon}_0$	The strain-rate at the reference stress σ_0

$\dot{a}$	The steady state crack velocity
$\hat{C}_k$	The separation history function of model k
λ	The characteristic geometric length scale
$(\bullet)^{\mathrm{cr}}$	The creep component of the quantity $(\bullet)$
$(\bullet)^{\mathrm{el}}$	The elastic component of the quantity $(\bullet)$
ω	A scalar damage parameter
$\overset{\triangledown}{a}$	The dimensionless steady state crack velocity
ϕ_0	The ratio of geometric to material length scales
σ_0	The reference stress
σ_{e}	The von Mises equivalent stress
σ_{ij}	The Cauchy stress tensor
ε_{ij}	The engineering strain tensor
a	The crack length
C^*	The rate of the J-integral
C_s	The separation history function of the simple model
E	Young's modulus
f	The current area fraction of the pores
f_0	The initial area fraction of the pores
f_{c}	The coalescence area fraction of the pores
h	The current height of a pore
h_0	The initial height of the pores
m	The rate sensitivity exponent of the damage zone
n	The rate sensitivity parameter of the bulk material
n_i	The unit normal vector ($i = 1, 2, 3$)
s_{ij}	The deviatoric part of Cauchy stress tensor
T_i	The traction vector ($i = 1, 2, 3$)
T_0	The reference traction of the damage zone
u_i	The displacement vector ($i = 1, 2, 3$)
x_i	The Cartesian material and spatial coordinates ($i = 1, 2, 3$)

1 Introduction

At elevated temperature, creep crack growth (CCG) is one of the most common failure mechanisms in many engineering applications, e.g. structural components, similar and dissimilar metal welds etc. This problem has received much attention over the last forty years due to the importance in designing structures with high integrity and safety. Hence, developing analytical models for steady-state crack growth which can be calibrated against detailed Finite Element models is of great interest. Further, an assessment of the effect of different material parameters and damage development processes on the crack growth behaviour can be provided using such models.

Studying creep crack growth has a long history in the literature. A major feature of these studies is the development of a parameter that characterizes the crack tip fields as well as crack propagation. Under steady state creep conditions, the so called C^*-integral (Landes and Begley 1976; Nikbin et al. 1976; Ohji et al. 1976) (i.e. the creep J-integral, Rice 1978) can be used to characterize the crack tip fields and creep crack growth. It provides descriptions of the strain-rate and stress singularities at the crack tip and a correlation of experimental crack growth rate data (Taira et al. 1979; Riedel and Rice 1980). Moreover, the C^*-integral is path independent for contours in which the material properties only vary in the direction perpendicular to the direction of crack growth within the family of contours considered. Riedel and Rice (1980) studied the transition from short-time elastic to long-time creep behaviour assuming that primary creep is negligible (small-scale creep conditions). They introduced a parameter $C(t)$ that describes the strain, strain-rate and stress fields within a creep zone that forms about the crack tip. Their analysis also provides a characteristic time for the transition to the steady state stress field (i.e. the time for $C(t)$ to equal C^*). Later, Ehlers and Riedel (1981) proposed a relation between $C(t)$ and C^*. Saxena (1986) proposed a new parameter C_{t} which can be measured easily in comparison with $C(t)$. Bassani et al. (1988) compared these two parameters and concluded that C_{t} characterizes crack growth rates much better than $C(t)$. Further, the $C(t)$ parameter is found to be more suitable for characterizing a stationary crack and C_{t} is related to a rapidly propagating crack. In the primary creep regime, Riedel (1981) suggested a new parameter C_h^* as an analogy to the C^*-integral. Further, Leung and McDowell (1990) included the primary creep effects in the estimation of the C_{t} parameter. To this end, the C^*, $C(t)$, C_{t} and C_h^* parameters are generally accepted and widely used in studying creep crack growth.

Under creep conditions, cracks in polycrystalline materials advance as a result of the growth of damage ahead of the crack tip (generally in the form of discrete voids or microcracks, which form primarily at grain boundaries). In the vicinity of a macroscopic primary crack tip, secondary micro-cracks are formed as a result of intensive void growth and coalescence and/or an accumulation and growth of micro-cracks. These secondary cracks propagate and coalesce creating the new crack surfaces, allowing the primary macroscopic crack to advance along an interface or interconnected grain-boundaries. The growth of damage can influence the constitutive properties of the material and therefore the details of the near crack tip stress and strain-rate fields. Early models of creep crack growth either assumed that the stress (e.g. Riedel 1981; Tvergaard 1984) or strain-rate field (e.g. Cocks and Ashby 1981; Nikbin et al. 1984) is the same as that for the undamaged material and used either empirical or mechanistic damage growth laws to determine the crack growth rate. In the strain based models the critical damage at the crack tip is expressed in terms of a material ductility (strain to failure) which is a function of the local stress state. Extensions of this approach within a finite element framework (employing models in which the constitutive relationships for deformation are not influenced by the presence of damage) have been undertaken by Nikbin et al. (1976, 1984), Yatomi and Nikbin (2014). Studies of the influence of damage on the nature of the crack tip fields and crack growth process where damage influences the deformation response have been undertaken by Riedel (1987) and Bassani and Hawk (1990) for empirical Kachanov (Kachanov 1958; Rabotnov 1969) type continuum damage mechanics models. More recently, the full interaction between deformation and damage development and how this influences the crack growth process has been modelled directly using the finite element method, using both mechanistic and empirical models for the growth of damage (e.g. Onck and van der Giessen 1998; Wen and Shan-Tung 2014).

In each of the above referenced studies damage development and its influence on crack growth is modelled as a continuum process. Another method of modelling crack propagation is through the use of interface cohesive or damage zone models. Interface damage zone models of this type provide a coupling between the local separation rate across an interface and bulk deformation processes, i.e. they introduce a physically meaningful length scale that is related to the dissipative mechanisms responsible for damage development. A damage zone model of this type describes the fracture process in the vicinity of the crack tip as a gradual surface separation process, such that the normal and shear tractions at the interface resist separation and relative sliding. The cohesive/damage zone modelling approach has its origins in the pioneering work of Dugdale (1960) and Barenblatt (1962). The first use of cohesive zone models in a finite element environment was undertaken by Hillerborg et al. (1976). Several models have been proposed in the literature, wherein a variety of materials and applications have been successfully investigated (Camacho and Ortiz 1996; Elmukashfi and Kroon 2014; Hui et al. 1992; Knauss 1993; Needleman 1987, 1990; Rahul-Kumar et al. 1999; Rice and Wang 1989; Tvergaard 1990; Xu and Needleman 1993). Rate-dependent and rate-independent models as well as physically based and phenomenological models have been employed. However, to the authors' knowledge, apart from the work of Onck and van der Giessen (1998), van der Giessen and Tvergaard (1994), Thouless et al. (1983) and Yu et al. (2012) damage zone type models have not been used to study the development of creep damage and/or creep crack growth.

In this paper, a theoretical and computational framework for creep crack growth is presented in which we assume that all the damage is concentrated in a narrow zone directly ahead of the growing crack tip. The objective is to model crack propagation in materials that exhibit steady state creep behaviour outside of the damage zone and to investigate the effect of different material parameters, forms of damage zone constitutive law and damage development processes on the crack growth behaviour. A theoretical framework is initially introduced in which the constitutive behaviour of the bulk material is described by power-law creep. A new class of damage zone model is proposed to model the fracture process such that the constitutive relation is described by a traction-separation rate law. More specifically, three different models, i.e. a simple critical displacement model, Kachanov type empirical models and a micromechanical based interface model are investigated, which mirror the types of models employed in the continuum models of creep crack growth described above. We follow the recent approach of Wang et al. (2016), who studied cleavage failure in creeping polymers, in which we keep the

material descriptions and geometric configurations as simple as possible to explore the relationship between the form of the constitutive model, material parameters and crack growth. With this in mind, we concentrate initially on the behaviour of a double cantilever beam specimen (DCB) of infinite length subjected to a constant pure bending moment, in which C^* remains constant as the crack grows and the crack growth rate eventually achieves a steady-state. We concentrate on the behaviour in the steady state. By invoking the path independence of the C^*-integral and choosing contours in the far field and surrounding the damage zone we demonstrate how a simple analytical expression for the crack growth rate can be obtained in terms of C^*, damage zone material parameters and a dimensionless scaling parameter that is a function of the ratio of characteristic geometric and material length scales, that can be determined using the finite element method. The theoretical framework is presented in Sect. 2. The analysis of creep crack growth in the double cantilever beam specimen and the finite element implementation of the damage zone model are described in Sect. 3, with the crack growth results for the different interface models presented and discussed in Sect. 4.

2 Theoretical framework for creep crack

2.1 Background

Consider a solid containing a stationary crack that is subjected to a constant load. The solid is assumed to exhibit elastic behaviour, together with primary, secondary and tertiary creep. Creep deformation evolves with increasing time and this evolution can be divided into different distinct stages. These stages have been described and evaluated by Bassani and Hawk (1990). Initially, a small-scale creep zone, i.e. small in comparison with the physical characteristic length of the body, is formed in the vicinity of the crack tip. In this stage, the material deforms by primary creep inside the creep zone and remains elastic elsewhere. Following the development of the primary creep zone, a secondary (steady-state) creep zone develops as a smaller region inside the primary creep zone. Thereafter, the primary and secondary creep zones continue to expand at the cost of the elastic and primary zones, respectively. During this process, damage accumulates in the crack tip region, which may lead to crack propagation if a critical condition is met. Hence, crack propagation may take place at different instants during the evolution of the near tip stress and strain-rate fields. The crack propagation scenarios are characterized by the nature of the crack tip fields at these instants: (i) the small-scale creep zone is formed surrounded by the elastic medium, (ii) the primary creep zone is large enough but remains surrounded by the elastic medium, (iii) the secondary creep zone is formed inside the primary creep zone but both zones remain surrounded by the elastic medium, (iv) the secondary creep zone is expanding inside the primary creep zone which dominates, (v) the secondary creep zone dominates.

This study concerns crack propagation in creeping materials under steady state conditions (type v). In this case, the C^*-integral can be used to characterize the creep crack growth behaviour. Note also, that as a crack grows in an elastic/creeping material, in the absence of damage, a zone develops ahead of the crack tip in which the stresses are determined by the elastic and creep properties of the material (Hui and Riedel 1981) who's size is a function of the crack velocity. For steady state behaviour the size of this zone must be small compared to the size of the crack tip damage process zone. Under these conditions, the path independent property can be used to obtain a direct relationship between the far field loading and the fracture process parameters.

In the following sub-sections we describe the constitutive relationships for the bulk continuum response and introduce a number of different models to describe the response ahead of the crack tip within the damage zone. We concentrate on mode I crack growth and only present relationships for the opening mode, although a description of the shear response is also required for the computational studies presented later. We consider the crack growth process in Sect. 3, where we use the path independence of the C^*-integral to relate the near crack tip damaging processes to the far field loading. In the theoretical models presented below we concentrate on steady state crack growth, where creep dominates the material response, i.e. we need not consider the elastic response. Similarly we do not need to consider any elastic/reversible contributions to the deformation within the damage zone.

2.2 Creep deformation and characterization of the remote field

Consider a body containing a crack and subjected to a constant far field loading, see Fig. 1. A common Cartesian coordinate system for the reference and deformed configurations x_i, $i = 1, 2, 3$, is assumed. The bulk material is assumed to exhibit steady-state creep behaviour and is defined by the constitutive law

$$\dot{\varepsilon}_{ij} = \frac{\partial \phi}{\partial \sigma_{ij}} = \frac{3}{2}\,\dot{\varepsilon}_0 \left(\frac{\sigma_\mathrm{e}}{\sigma_0}\right)^n \frac{s_{ij}}{\sigma_\mathrm{e}}, \tag{1}$$

where σ_{ij} is Cauchy's stress tensor, $\dot{\varepsilon}_{ij}$ is the strain rate tensor, $s_{ij} = \sigma_{ij} - \frac{1}{3}\sigma_{kk}\delta_{ij}$ is the stress deviator, $\sigma_\mathrm{e} = \sqrt{\frac{3}{2}s_{ij}s_{ij}}$ is the von Mises equivalent stress, σ_0 is a reference stress, $\dot{\varepsilon}_0$ is the strain-rate at the reference stress and n is the rate sensitivity parameter. ϕ is the stress potential

$$\phi = \frac{1}{n+1}\,\dot{\varepsilon}_0\sigma_0 \left(\frac{\sigma_\mathrm{e}}{\sigma_0}\right)^{n+1}. \tag{2}$$

The energy dissipation rate, $\dot{D}$, is given by

$$\dot{D} = \phi + \psi, \tag{3}$$

where ψ is the dual rate potential

$$\psi = \frac{n}{n+1}\,\dot{\varepsilon}_0\sigma_0 \left(\frac{\dot{\varepsilon}_\mathrm{e}}{\dot{\varepsilon}_0}\right)^{\frac{n+1}{n}}, \tag{4}$$

and $\dot{\varepsilon}_\mathrm{e} = \sqrt{\frac{2}{3}\dot{\varepsilon}_{ij}\dot{\varepsilon}_{ij}}$.

Crack propagation is assumed to be determined by an interface model such that the propagation takes place along a fictitious interface surface, Γ_int. As the crack advances separation occurs along the interface to create two surfaces. Hence, a material point along the interface is defined by the two normal vectors n_i^- and n_i^+, where $n_i^- = -n_i^+$, i.e. the initially intact material point splits into two points with unit normals acting opposite to each other and into the material on either side of the interface. The displacement-rate jump across the damage zone surface and the corresponding tractions are defined by the vectors $\delta_i = u_i^+ - u_i^-$, where u_i^+ and u_i^- are the displacement rates either side of the interface, and $T_i^+ = \sigma_{ij}\, n_j^+$, $T_i^- = \sigma_{ij}\, n_j^-$.

In order to analyse the problem the C^*-integral is determined on the inner and the outer contours in Fig. 1.

The C^*-integral is defined as

$$C^* = \int_\Gamma W \cdot \mathrm{d}x_2 - T_i \frac{\partial \dot{u}_i}{\partial x_1} \cdot \mathrm{d}s, \tag{5}$$

where Γ is an arbitrary contour around the tip of the crack with unit outward normal n_i, $T_i = \sigma_{ij}\, n_j$ is the traction on $\mathrm{d}s$ and $\dot{u}_i$ is the displacement rate. The C^*-integral in the outer path, C^*_out, is determined by the far field loading. We consider the situation where a damage zone extends along the x_1 axis directly ahead of the crack tip, see Fig. 2. The first term of Eq. (5) then vanishes, since $\mathrm{d}x_2 = 0$. The contribution of the damage region to the C^*-integral along the inner path, C^*_in, is then evaluated as

$$\begin{aligned} C^*_\mathrm{in} &= -\int_{\Gamma_\mathrm{in}} T_i \frac{\partial \dot{u}_i}{\partial x_1} \cdot \mathrm{d}s \\ &= -\int_0^L \sigma_{ij} n_i^- \frac{\partial \dot{u}_i^-}{\partial x_2} \cdot \mathrm{d}x_1 + \int_L^0 \sigma_{ij} n_i^+ \frac{\partial \dot{u}_i^+}{\partial x_1} \cdot \mathrm{d}x_1 \\ &= -\int_0^L \sigma_{ij} n_i^+ \frac{\partial \dot{\delta}}{\partial x_1} \cdot \mathrm{d}x_1 \\ &= \int_0^{\dot{\delta}_i^m} \sigma_{ij} n_i^+ \cdot \mathrm{d}\dot{\delta}_i = \int_0^{\dot{\delta}_i^m} T_i^+ \cdot \mathrm{d}\dot{\delta}_i, \end{aligned} \tag{6}$$

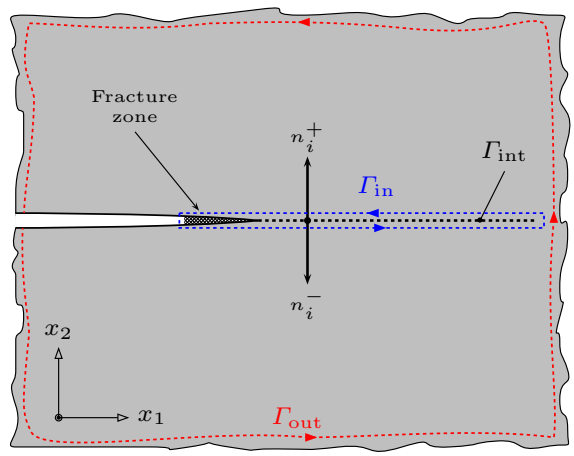

Fig. 1 The schematic of interface crack model in creeping solid. The figure illustrates the definition of the interface surface Γ_int. inner path Γ_in and the outer path Γ_out

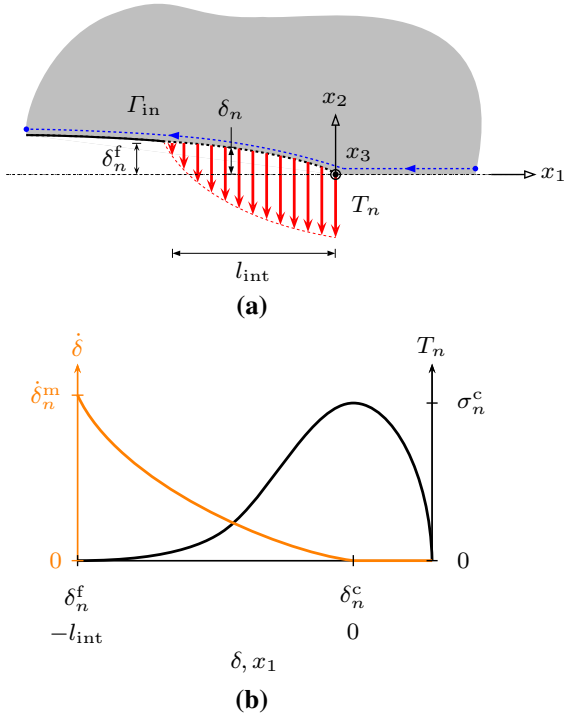

Fig. 2 The cohesive zone for pure mode I crack propagation: **a** schematic of the cohesive zone; and **b** the normal traction-separation ($T_n - \delta_n$) and the separation rate-separation ($\dot{\delta}_n - \delta_n$) distribution along the cohesive zone. l_{int} is the length of the cohesive zone, δ_n^{c} is the critical displacement, δ_n^{f} is the displacement at failure, and σ_n^{c} is the cohesive strength

where $\dot{\delta}_n^{\text{m}}$ is the opening rate at the tip of the crack. In order to simplify the relationships used in subsequent analysis we omit the superscript "+" from the traction. Using the path-independence property of C^* (ie, $C^*_{\text{out}} = C^*_{\text{in}}$) provides a relationship between the far field loading and the behaviour within the damage zone. In order to complete the analysis we need a constitutive relationship for the damage zone that relates $\dot{\delta}_i$ to T_i. In this paper we concentrate on mode I loading and therefore only need to consider the components of traction and displacement-rate normal to the damage zone. Then

$$C^*_{\text{in}} = \int_0^{\dot{\delta}_n^{\text{m}}} T_n \cdot \mathrm{d}\dot{\delta}_n. \tag{7}$$

In the following sub-section we present a number of different constitutive relationships for the damage zone response.

2.3 Damage zone models for creep crack growth

In this section, we present models for the damage zone. We limit our description to mode I loading. More general relationship for mode II and mixed mode loading are described elsewhere (Elmukashfi and Cocks 2017). For each of the models here we assume that the relationship between $\dot{\delta}_n$ and T_n can be expressed in the form of a power-law. Further, these models are capable of predicting similar damaging processes and crack growth behaviour through the appropriate selection of material parameters, see "Appendix B".

2.3.1 Simple critical displacement model

The simplest form of traction-separation rate law is defined by a direct power-law relationship between the normal traction T_n and the separation rate $\dot{\delta}_n$. Further, damage does not influence the opening rate and failure is achieved when δ_n achieves a critical separation δ_n^{f}. Thus, the constitutive model takes the following form

$$\dot{\delta}_n = \dot{\delta}_0 \left(\frac{T_n}{T_0} \right)^m, \tag{8}$$

where T_0 is a reference traction (equivalent to of Eq. (1), $\dot{\delta}_0$ is the separation rate at this traction and m is an exponent which can have a different value to n in Eq. (1). It should be noted that the traction becomes zero when the separation exceeds the critical value, i.e. $T_n = 0$ if $\delta_n \geq \delta_n^{\text{f}}$.

2.3.2 Kachanov damage type empirical model

In this model damage is assumed to influence the constitutive response and a single scalar damage parameter ω is introduced to incorporate the effect of damage. The damage parameter is assumed to evolve monotonically from 0 to 1, i.e. from an undamaged to a fully damaged state. Following Kachanov (1958) and Lemaitre and Chaboche (1994) we assume that the separation rate is a function of an effective traction $\bar{T}_n$, which is related to the normal traction T_n and ω by

$$\bar{T}_n = \frac{T_n}{1 - \omega}. \tag{9}$$

The constitutive response is then simply obtained by replacing T_n by $\bar{T}_n$ in Eq. (8) to give

$$\dot{\delta}_n = \dot{\delta}_0 \left(\frac{T_n}{(1-\omega)\ T_0} \right)^m . \tag{10}$$

The damage is assumed to be determined by the normal separation δ_n, i.e. $\omega = \omega(\delta_n)$, and the damage evolution law may take different forms depending on the damage mechanism(s). In this study, we propose two different damage models, namely linear and exponential models. The different evolution laws are:

– The linear damage model:

$$\omega = \begin{cases} \dfrac{\delta_n - \delta_n^{\mathrm{c}}}{\delta_n^{\mathrm{f}} - \delta_n^{\mathrm{c}}} & \text{if } \delta_n \geq \delta_n^{\mathrm{c}}, \\ 0 & \text{if } \delta_n < \delta_n^{\mathrm{c}}. \end{cases} \tag{11}$$

– The exponential damage model:

$$\omega = \begin{cases} 1 - \exp\left[-\beta \left(\dfrac{\delta_n - \delta_n^{\mathrm{c}}}{\delta_n^{\mathrm{f}} - \delta_n^{\mathrm{c}}} \right) \right] & \text{if } \delta_n \geq \delta_n^{\mathrm{c}}, \\ 0 & \text{if } \delta_n < \delta_n^{\mathrm{c}}. \end{cases} \tag{12}$$

where δ_n^{c} is the separation at which damage initiates (for separations less than this value $\omega = 0$ and the constitutive response is given by Eq. (1)), as before δ_n^{f} is the separation at failure and β is a material parameter. It should be noted that for the exponential damage law the traction does not necessarily decrease smoothly to zero at failure but an abrupt response may result. Figure 3 below shows the traction-separation law for different separation rates for the case of linear and exponential damage laws.

2.3.3 Micromechanical based model

This model is based on the creep extension of Yalcinkaya and Cocks (2015) micromechanical damage zone model for ductile fracture described by Cocks et al. (2017), which are both derived from the creep cavitation model of Cocks and Ashby (1980). These models are based on the growth of an array of pores idealized as cylinders. The relation between the macroscopic traction and separation and the microscopic stress and strain is then obtained using classical bounding theorems.

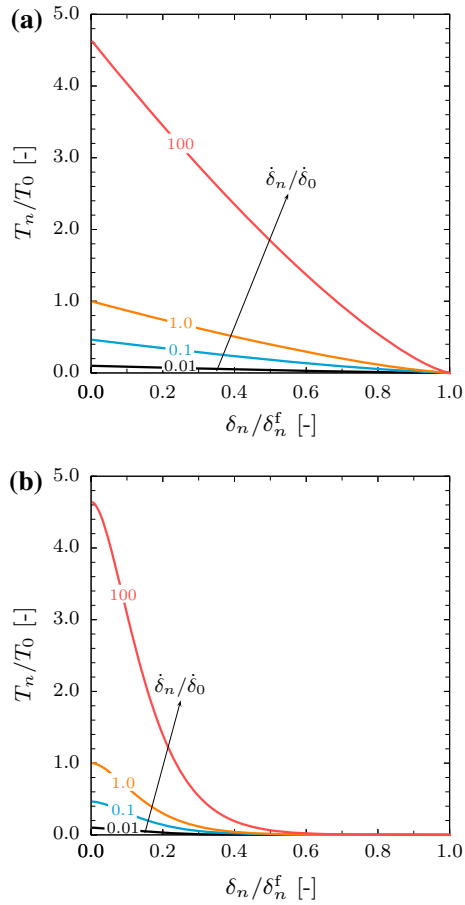

Fig. 3 The Kachanov damage type model traction-separation rate law: **a** the linear damage model and **b** the exponential damage model. The rate sensitivity exponent is taken to be $m = 9$

The radius and height of the pores at a given instant are denoted as r and h, respectively, and the mean spacing is $2l$, see Fig. 4. Thus, the pores are characterized by their area fraction in the plane of the cavitated zone, i.e. by $f = (r/l)^2$. Further, the representative volume element is assumed to be fully constrained in the radial direction and the deformation is only controlled by the normal separation, i.e. $l = \text{const.}$ and $\dot{h} = \dot{\delta}_n$. This simplification of the void profile captures the major features of the evolving geometry (such as area fraction of pores and pore aspect ratio) while allowing simple analytical expressions for the evolution of damage to be derived. More general forms of model are discussed by Cocks et al. (2017)—this is the simplest form of model of this class and it is directly equivalent in form to classical rate dependent cohesive zone models, including those described above. The resulting expression for the

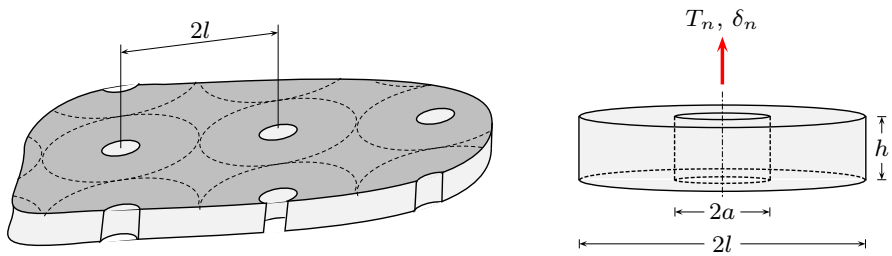

(a) **(b)**

Fig. 4 The micromechanical representation of the creep damage by pore growth: **a** pores of radius r and spacing $2l$ on a grain boundary subjected to microscopic stress state σ_{ij} and the deformation is controlled by steady-state creep and **b** an idealization of a pore as a cylinder with height h and diameter equal to the pore to pore spacing $2l$ and the macroscopic normal traction T_n and separation δ_n

opening rate is

$$\dot{\delta}_n = \dot{\delta}_0 \frac{1}{\bar{g}_n} \left(\frac{T_n}{\bar{g}_n T_0} \right)^m , \tag{13}$$

where $\bar{g}_n = g_n(f)/g_0$ and

$$g_n = \left[(1-f)^2 + \left(\frac{1}{\sqrt{3}} \ln \frac{1}{f} \right)^2 \right]^{\frac{1}{2}} . \tag{14}$$

and g_0 is a parameter that can be used to provide a similar rupture time to the Kachanov models under the same stress level and the same value of the material parameters $\dot{\delta}_0$, T_0 and δ_n^{f} (see "Appendix B"). The matrix material is incompressible, therefore the total rate of change in volume is equal to the rate of change in pore volume. Hence, the pore area fraction evolves at a rate

$$\dot{f} = \frac{\dot{\delta}_n}{h} (1-f) . \tag{15}$$

The initial pore area fraction and height are assumed to be f_0 and h_0, respectively. Further, the pores are assumed to coalesce and reach a complete failure when $f = f_{\mathrm{c}}$. The direct integration of Eq. (15) gives the separation at failure:

$$\int_{f_0}^{f_{\mathrm{c}}} \frac{1}{(1-f)} \cdot \mathrm{d}f = \int_{h_0}^{h} \frac{1}{h} \cdot \mathrm{d}h \implies \delta_n^{\mathrm{f}} = h_0 \left[\frac{1-f_0}{1-f_{\mathrm{c}}} - 1 \right] . \tag{16}$$

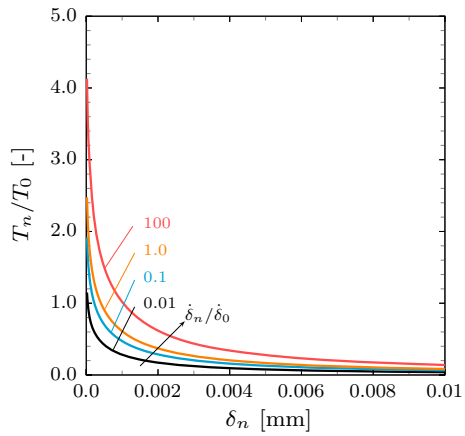

Fig. 5 The micromechanical based model traction-separation rate law. The initial pore area fraction and height are assumed to be $f_0 = 0.01$ and $h_0 = 0.001$ mm

The traction-separation rate relation for different separation rates is illustrated in Fig. 5.

3 Creep crack growth in a double cantilever beam

In this section, pure mode-I creep crack growth in the DCB specimen shown in Fig. 6 is analysed. The length and height, of the specimen are denoted by L and $2H$, respectively, and the crack length is denoted by a. Each arm of the specimen is subjected to a constant moment M per unit depth. We assume that the overall length $L \longrightarrow \infty$ and that the height of each arm $H \ll a$. Under these conditions C^*, remains constant as the crack grows, thus a steady state is eventually achieved in which the crack growth rate is constant. We focus on this steady state response. The objective is to obtain a

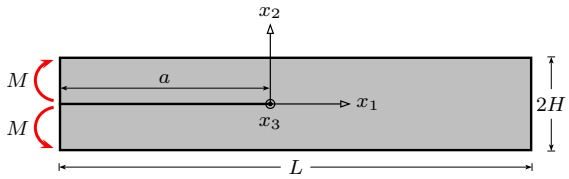

Fig. 6 The schematic of the double cantilever beam specimen

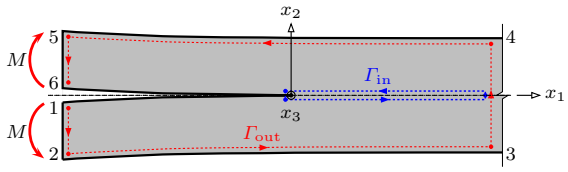

Fig. 7 The definition of the *inner path* Γ_{in} and the *outer path* Γ_{out} that are used to evaluate the C^*-integral in the double cantilever beam specimen

mathematical description for the relationship between the far field loading and the local damage development within the damage zone and the crack growth rate under both plane stress and plane strain conditions.

In order to determine the relationship between the loading and fracture parameters, the path independence of the C^*-integral is used as discussed in Sect. 2. The C^*-integral is evaluated along the outer and inner paths indicated by the dashed lines and different colours in Fig. 7. Equating the values of C^* determined from these two paths provides a relationship between the crack-tip opening rate and the applied load. There is a single characteristic geometric length scale for this problem, which we take as $\lambda = H/2$, and in the steady state the separation rate within the damage zone can be expressed as a function of x_1/λ, integrating this function as an element is convected towards the crack tip as the crack grows at constant velocity, allows the crack growth rate to be determined. We do not know the form of this function a priori, but to determine the crack growth rate we only need to determine a single quantity—the resulting integral, which can be determined from a single piece of information from a finite element analysis of the problem. The details of this process are given below.

3.1 The C^*-integral in the outer path Γ_{out}

C^* in the outer path can be determined in a number of different ways—for example by direct evaluation of the integral of Eq. (5) or by determining the rate of change of the rate analogue of the total potential energy, Π, with crack length, where

$$\Pi = \int_V \psi \cdot dV - \int_S T_i \dot{u}_i \cdot \mathrm{d}S. \tag{17}$$

We adopt the second of these approaches here. For an element of beam under bending the curvature rate is given by

$$\dot{\kappa} = \frac{2\dot{\varepsilon}_0}{H}\left(\frac{2n+1}{2n}\,\frac{4M}{\sigma_0 H^2}\right)^n = \frac{2\dot{\varepsilon}_0}{H}\eta\left(\frac{\eta M}{M_0}\right)^n, \tag{18}$$

where $M_0 = \dfrac{2n}{2n+1}\,\dfrac{\sigma_0 H^2}{4}$, and $\eta = 1$ for plane stress and $\sqrt{3}/2$ for plane strain. For the DCB specimen of Fig. 7

$$\begin{aligned} C^*_{\text{out}} &= -\left.\frac{\partial \Pi}{\partial a}\right|_M \\ &= 2\left[\frac{n}{n+1}\frac{2\dot{\varepsilon}_0}{H}M_0\left(\frac{\dot{\kappa}H}{2\dot{\varepsilon}_0}\right)^{\frac{n+1}{n}} - M\frac{\partial \dot{\theta}}{\partial a}\right] \\ &= 2\left[\frac{n}{n+1}\frac{2\dot{\varepsilon}_0}{H}M_0\left(\frac{\dot{\kappa}H}{2\dot{\varepsilon}_0}\right)^{\frac{n+1}{n}} - M\dot{\kappa}\right] \\ &= \frac{2}{n+1}\frac{2\dot{\varepsilon}_0}{H}M_0\left(\frac{\eta M}{M_0}\right)^{n+1}. \end{aligned} \tag{19}$$

The factor of 2 arises because there are 2 beams and $\dot{\theta}$ is the rotation rate at the end of one of the beams. If we define a reference stress, such that

$$\sigma_0 = \frac{2n+1}{2n}\,\frac{4\eta M}{H^2}, \tag{20}$$

and

$$C^*_{\text{out}} = f_n(n)\,\dot{\varepsilon}_0\sigma_0\lambda, \tag{21}$$

where $f_n(n) = \dfrac{4n}{(2n+1)(n+1)}$ and $\lambda = H/2$ is the characteristic length scale for the DCB specimen.

3.2 The C^*-integral in the inner path Γ_{in}

Using the definition in Eq. (7), the C^*-integral in the inner path Γ_{in} can be written as

$$C^*_{\text{in}} = \int_0^{\dot{\delta}^{\text{m}}_n} T_n \cdot \mathrm{d}\dot{\delta}_n = \int_0^{\dot{\delta}^{\text{m}}_n} d_k \, T_0 \left(\frac{\dot{\delta}_n}{\dot{\delta}_0}\right)^{\frac{1}{m}} \cdot \mathrm{d}\dot{\delta}_n, \tag{22}$$

where the function d_k depends on the form of interface model adopted, with k indicating the model, i.e. s $\equiv$ simple, kl $\equiv$ Kachanov linear, ke $\equiv$ Kachanov exponential and m $\equiv$ micromechanical models. For each of these models d_k is given by

$$d_{\text{s}} = 1, \quad d_{\text{ke}} \text{ and } d_{\text{ke}} = 1-\omega \quad \text{and} \quad d_{\text{m}} = g_n^{\frac{m+1}{m}}. \tag{23}$$

Apart for the simple model the integral requires a knowledge of the stress history experienced by each material point in the damage zone, which is not known a priori. For the simple model the integral of Eq. (22) can be readily determined:

$$C^*_{\text{in}} = \int_0^{\dot{\delta}^{\text{m}}_n} T_0 \left(\frac{\dot{\delta}_n}{\dot{\delta}_0}\right)^{\frac{1}{m}} \cdot \mathrm{d}\dot{\delta}_n = \frac{2m}{m+1} \, \dot{\delta}_0 \, T_0 \left(\frac{\dot{\delta}^{\text{m}}_n}{\dot{\delta}_0}\right)^{\frac{m+1}{m}}. \tag{24}$$

For all the remaining models $0 \le d_k \le 1$, and the resulting integral is therefore less than or equal to that given by Eq. (24). We assume that the integral for each model can be approximated by

$$\begin{aligned} C^*_{\text{in}} &= \alpha_k \int_0^{\dot{\delta}^{\text{m}}_n} T_0 \left(\frac{\dot{\delta}_n}{\dot{\delta}_0}\right)^{\frac{1}{m}} \cdot \mathrm{d}\dot{\delta}_n \\ &= \alpha_k \, \frac{2m}{m+1} \, \dot{\delta}_0 \, T_0 \left(\frac{\dot{\delta}^{\text{m}}_n}{\dot{\delta}_0}\right)^{\frac{m+1}{m}}, \end{aligned} \tag{25}$$

where the subscript k again identifies the model and α_k falls in the range $0 \le \alpha_k \le 1$.

3.3 The crack tip opening displacement rate

Equating the values of C^* given by the inner and outer contours, i.e. Eqs. (21) and (25), allows the crack tip opening displacement rate $\dot{\delta}^{\text{m}}_n$ to be expressed as a function of the applied loading. Equating T_0 to σ_0 gives

$$\dot{\delta}^{\text{m}}_n = \dot{\delta}_0 \left(\frac{q\,(n,m)\;\phi_0}{\alpha_k}\right)^{\frac{m}{m+1}}, \tag{26}$$

where $\phi_0 = \dfrac{\dot{\varepsilon}_0 \, \lambda}{\dot{\delta}_0} = \dfrac{\dot{\varepsilon}_0 \, H}{2\dot{\delta}_0}$ is the ratio of geometric to material length scales for the problem and $g\,(n,m) = f_n\,(n) \cdot \dfrac{m+1}{2m} = \dfrac{2n\,(m+1)}{m\,(2n+1)\,(n+1)}$, which for $n = m$ reduces to $q\,(n,n) = q_n\,(n) = \dfrac{2}{2n+1}$.

3.4 The analysis of a steadily propagating crack

As noted earlier, under a constant applied moment the crack velocity will, after an initial transient, achieve a steady state, in which it reaches a constant value $\dot{a}$. We consider a coordinate system that moves with the crack tip. A material element such as P in Fig. 8a then moves along the x_1-direction at a rate (Cocks and Ashby 1981)

$$\frac{\mathrm{d}x_1}{\mathrm{d}t} = -\dot{a}. \tag{27}$$

The are two characteristic length scales in this problem, the geometric length scale λ and the material length scale $\dot{\delta}_0/\dot{\varepsilon}_0$. We can therefore write the separation rate in the form

$$\dot{\delta}_n = \dot{\delta}^{\text{m}}_n \cdot \Lambda_k \left(\frac{x_1}{\lambda}\right) = \dot{\delta}^{\text{m}}_n \cdot \Lambda_k \left(\bar{x}_1\right), \tag{28}$$

where Λ_k is a dimensionless function that depends on the interface model whose detailed form depends on ϕ_0, the ratio of geometric and material length scales, as shown in Fig. 8b. For each of the models described in Sect. 2, failure of an element occurs when the separation across the damage zone reaches a critical value, δ^{f}_n. Integrating the displacement rate as an element is convected towards the crack tip gives

$$\begin{aligned} \delta^{\text{f}}_n &= \int_0^{t_{\text{f}}} \dot{\delta}_n \cdot \mathrm{d}t = -\int_{\infty}^{0} \dot{\delta}_n \cdot \frac{\mathrm{d}x_1}{\dot{a}} \\ &= \frac{\dot{\delta}^{\text{m}}_n \, \lambda}{\dot{a}} \int_0^{\infty} \Lambda_k \left(\bar{x}_1\right) \cdot \mathrm{d}\bar{x}_1 \\ &= \frac{\dot{\delta}^{\text{m}}_n \, \lambda}{\dot{a}} \, C_k \left(\phi_0, n, m\right), \end{aligned} \tag{29}$$

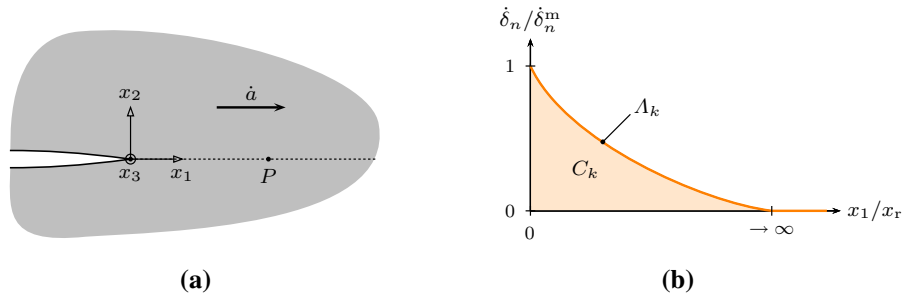

(a) **(b)**

Fig. 8 The schematics of a steadily propagating crack in viscous solid: **a** a material point P at distance x_1 from the moving crack tip and **b** the definition of the Λ_k and C_k dimensionless functions for point P

where we have used Eq. (27) to substitute for dt and Eq. (28) to substitute for $\dot{\delta}_n$. The dimensionless function $C_k\,(\phi_0, n, m)$ is only a function of ϕ_0, n, m and the detailed form of model for the damage zone. Substituting for $\dot{\delta}_n^{\mathrm{m}}$ using Eq. (24) gives the steady state crack velocity.

$$\overset{\triangledown}{a} = \frac{\dot{a}}{\dot{\varepsilon}_0\lambda} = q\,(n,m)^{\frac{m}{m+1}}\,\frac{\phi_0^{-\frac{1}{m+1}}}{\bar{\delta}_n^{\mathrm{f}}}\,\frac{C_k\,(\phi_0,n,m)}{\alpha_k^{\frac{m}{m+1}}}$$

$$= q\,(n,m)^{\frac{m}{m+1}}\,\frac{\phi_0^{-\frac{1}{m+1}}}{\bar{\delta}_n^{\mathrm{f}}}\hat{C}_k\,(\phi_0,n,m)\,. \tag{30}$$

where $\bar{\delta}_n^{\mathrm{f}} = \delta_n^{\mathrm{f}}/\lambda$. We can express this relationship in a number of different forms. An alternative form that can be used to provide some insight into the material response is:

$$\dot{a} = \frac{A^{\frac{1}{m+1}}\lambda}{\delta_n^{\mathrm{f}}}\left[\frac{m+1}{2m}C^*\right]^{\frac{m}{m+1}}\hat{C}_k\,(\phi_0,n,m) \tag{31}$$

where $A = \dot{\delta}_0/\sigma_0^m$ is a material constant for the damage zone [see Eq. (8)]. The form of this equation might suggest that the crack growth rate is a function of C^*, for a given value of δ_n^{f}. This is only true if $\hat{C}_k$ is only a function of n and m or ϕ_0 is constant for the range of conditions of interest. Note that for the DCB specimen of Fig. 7 and $m = n$

$$\phi_0 = \frac{B}{A}\lambda = \frac{B}{A}\frac{H}{2} \tag{32}$$

where $B = \dot{\varepsilon}_0/\sigma_0^m$ is a material property. Then for a series of experiments in which the geometry is kept constant we would expect $\dot{a}$ to be proportional to $C^{*\frac{m}{m+1}}$, but the constant of proportionality could be different for a different choice of beam height H. For more general cracked geometries σ_0, $\dot{\varepsilon}_0$ and λ change as a crack grows and therefore ϕ_0 also changes. This needs to be taken into account in any model and description of the crack growth process. We consider this feature of the response further below.

In order to determine the crack growth rate we need to evaluate the quantity $\hat{C}_k$. We can determine this using the finite element method. We need not determine the distributions d_k and Λ_k ahead of the crack tip. We can determine directly by equating the numerically determined crack velocity with the prediction of Eq. (30).

3.5 Numerical implementation of the governing equations

The initial-boundary value problem described in Sect. 3 is numerically solved using the FE (Finite Element) code ABAQUS (Abaqus 2016). A nonlinear quasi-static analysis is used for the initial loading, and a nonlinear visco analysis is used for the creep crack propagation analysis. In the visco analysis implicit time integration is used to solve the FE equations and mixed implicit/explicit integration is used for the integration of the creep and damage zone equations. The FE analysis requires the solution for an elastic/creep constitutive law in the bulk an elastic-rate dependent opening model for the damage zone. Elastic constitutive components have been added to the constitutive relationships of Eqs. (1), (8), (10) and (13), with the values of the elastic components chosen to have limited influence on the computed results.

The geometry of the double cantilever beam (DCB) specimen shown in Fig. 6 is discretised, and a typical finite element mesh is shown in Fig. 9. Only one half of the specimen is analysed due to the symmetry of the problem. The dimensions are taken as $L = 100$ mm, $H = 10$ mm, and $B = 1$ mm. The initial crack is assumed to be $a = 40$ mm, and the crack propagation

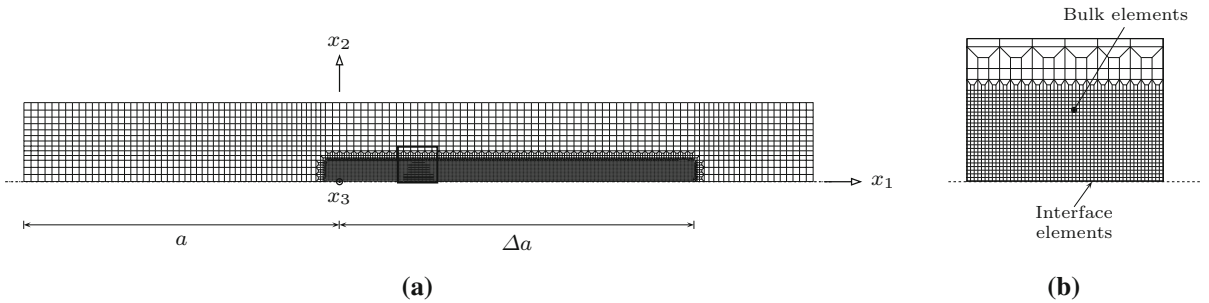

Fig. 9 The finite element mesh of the double cantilever beam specimen: **a** the mesh of the whole geometry; and **b** mesh details along the middle of the specimen where the cohesive elements are inserted along the crack propagation path

is studied over a length of $\Delta a = 50$ mm. The 4-node reduced integration bilinear plane stress and strain elements (CPS4R and CPE4R) are used in the discretisation for plane stress and strain conditions, respectively. A 4-node two-dimensional linear damage zone element was implemented in ABAQUS using the user-defined subroutine UEL. The details of the Finite Element implementation are provided in "Appendix A". The Finite Element model is divided into two regions, in which the bulk and damage zone elements are defined. The damage zone elements are inserted along the crack propagation path, i.e. along $a \leq x_1 \leq L$ and $x_2 = 0$, and the bulk elements are defined elsewhere. The top faces of the damage zone elements are attached to the bulk elements, see Fig. 9b.

The damage zone elements are modelled with zero initial thickness such that the top and bottom face nodes coincide. The mesh has 11,634 elements, of which 11,279 are bulk elements and 355 are damage zone elements. A uniform refined element region is created adjacent to the crack and its propagation for controlling the interface element length l_{inte}. A convergence study on the mesh refinement was carried out for different values of ϕ_0 and interface parameters $\bar{\delta}_n^{\text{f}} = 0.004$, $\beta = 1.0$, $f_0 = 0.01$ and $f_{\text{c}} = 0.91$. We found that an interface element length of $l_{\text{inte}} = 0.1$ mm is necessary to obtain converged solutions for the range $\phi_0 \in \left[10^{-5} - 10^{4}\right]$. The interface stiffness $K_n = K_t = 10^6$ MPa $\cdot$ mm is selected such that the elastic deformation is negligible (see "Appendix A").

The numerical analysis was performed for different combinations of the dimensionless parameters defined above to confirm that the functional form of Eq. (30) is valid. (The model parameters are chosen in such a way that the dimensionless parameters are controlled.) The relative normal separation displacement, Δu_2, between each pair of initially coincident nodes in the interface ($x_2 = 0$) is computed and recorded during the analysis. The crack tip position, x_{tip}, is defined by $\Delta u_2 = \delta_n^{\text{f}}$, and the crack tip velocity is determined using forward differencing as

$$v_{\text{tip}}^{p} = \left.\frac{\mathrm{d}x_{\text{tip}}}{\mathrm{d}t}\right|_{t_p} = \frac{x_{\text{tip}}^{p+1} - x_{\text{tip}}^{p}}{\Delta t_p} \tag{33}$$

where indices p and $p+1$ denote variable values at instants t_p and t_{p+1}, respectively, and $\Delta t_p = t_{p+1} - t_p$ is the time increment. Further, the steady crack velocity, $\dot{a}$, is computed by taking the average velocity over the steady propagation period.

4 Results and discussion

4.1 The crack growth

Several analyses have been performed for different combinations of the dimensionless parameters and damage zone properties. The crack tip position, transient and steady state crack propagation velocity have been obtained for all the combinations. For the simple interface model the parameters $n = m = 9$, $\phi_0 = 1.0$ and $\bar{\delta}_n^{\text{f}} = 0.004$ are used to illustrate the different results. We first describe the results under plane stress conditions.

Figure 10i–iv show the distribution of the effective creep strain $\dot{\varepsilon}_{\text{e}}^{\text{cr}}$ at four different instants and crack velocities. At $t = 0$ the creep deformation is zero everywhere and elastic deformation prevails. As time passes

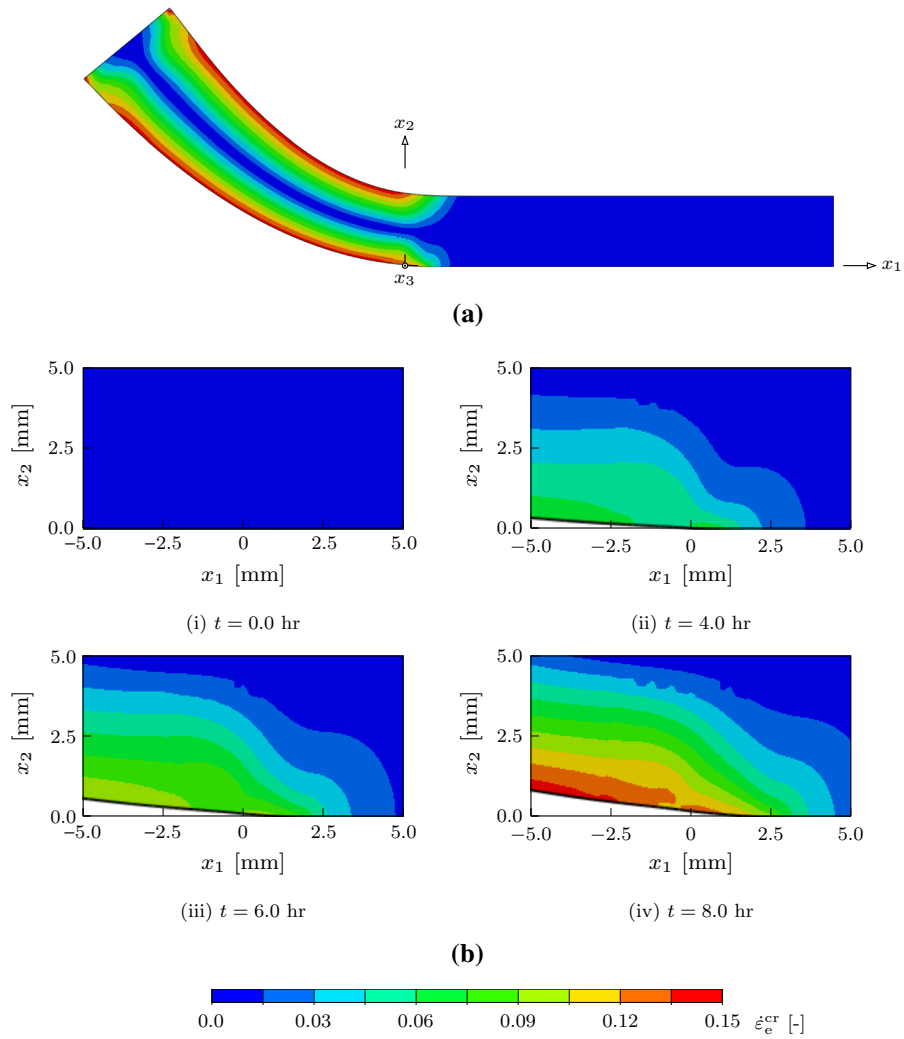

Fig. 10 The Distribution of the effective creep strain $\dot{\varepsilon}_e^{cr}$ for the parameters $n = m = 9$, $\phi_0 = 1.0$ and $\bar{\delta}_n^f = 0.004$: **a** the deformed DCB specimen at time $t = 8$ h; and **b** the propagating crack tip at different instants of time

($t > 0$) creep deformation evolves in the bulk, initially primarily in the vicinity of the crack tip, as well as damage along the interface, leading eventually to crack growth when the critical opening is achieved at the crack tip.

Figure 11a, b show the crack tip position and velocity as functions of time, respectively. The plots show that the crack starts to propagate slowly and accelerates to a high velocity and after a short time (10 h) a lower steady state velocity is achieved. In this case a steady velocity of $\dot{a} = 0.311$ mm/h is obtained. The result shows that the transient velocity is higher than the steady state velocity suggesting that the stress at the crack tip is initially high due to the elastic deformation and as the crack advances the creep deformation dominates where the stress relaxes leading to a slower propagation rate. Additionally the damage ahead of the crack tip is fully developed during both transient and steady propagation. The other scenario is when the damage is not fully developed during the transient stage which may lead to a slower propagation before reaching a steady state where a fully developed damage zone is achieved.

4.2 The C_s-function

It proves instructive to concentrate initially on the response for the simple damage zone model of Sect. 2.3.1. The Finite Element analysis is used to determine the steady crack velocity $\dot{a}$ and then for a given set of input parameters the C_s-function can be evaluated from Eq. (30):

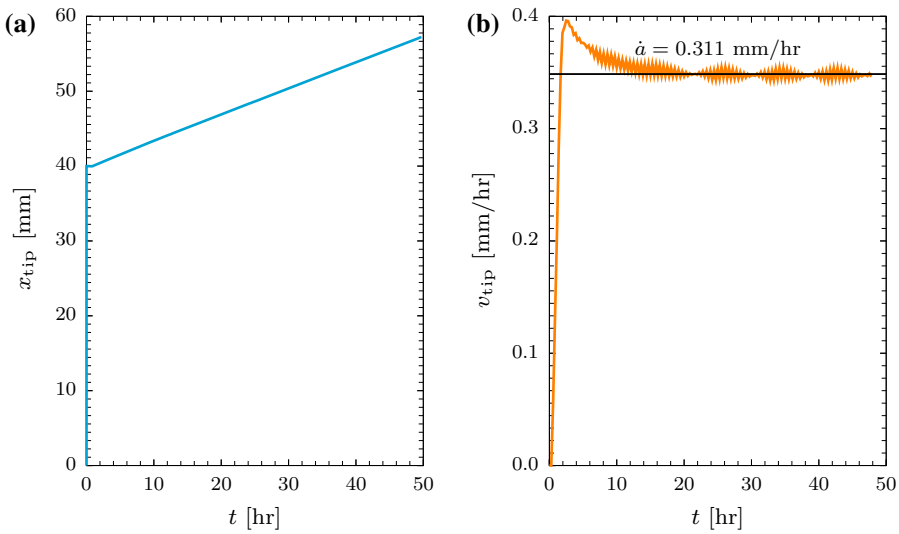

Fig. 11 Crack propagation results for $n = m = 9$, $\phi_0 = 1.0$ and $\bar{\delta}_n^{\rm f} = 0.004$: **a** crack tip position $x_{\rm tip}$ versus time t; and **b** crack tip velocity $v_{\rm tip}$ versus time t

$$\hat{C}_k = \frac{\overset{\triangledown}{a}\, \bar{\delta}_n^{\rm f}\, \phi_0^{\frac{1}{m+1}}}{g\,(n,m)^{\frac{m}{m+1}}}. \tag{34}$$

The appropriateness of the dimensionless analysis has been examined using the same set of dimensionless parameters with different model parameters, e.g. the same value of ϕ_0 with different combinations of$\dot{\varepsilon}_0$, H and $\dot{\delta}_0$.

4.3 The physical limits and the validity of the framework

Before evaluating the computational results in detail it is instructive to examine the response in the limits of small and large ϕ_0. The first extreme is when the interface is very stiff in comparison with the bulk material (the bulk material creeps faster than the interface, i.e. $\dot{\varepsilon}_0 \gg \dot{\delta}_0/\lambda$ and $\phi_0 \to \infty$). The other extreme occurs when the interface creeps faster than the bulk material, i.e. the interface is very compliant ($\dot{\varepsilon}_0 \ll \dot{\delta}_0/\lambda$ and $\phi_0 \to 0$). In this analysis we consider the simple damage zone model of Sect. 2.3.1.

When an interface is very stiff in comparison with the bulk material the deformation along the interface is negligible and it does not influence the stress state in the body. The tractions seen by the damage zone are determined by the stress distribution in the bulk material, and can be expressed in terms of the C^*-integral (provided the damage zone is small compared to the region in which the HRR field dominates; Hutchinson 1968; Rice and Rosengren 1968). The HRR stress field is defined as

$$\sigma_{ij} = \sigma_0 \left[\frac{C^*}{\dot{\varepsilon}_0\, \sigma_0\, I_n\, r}\right]^{\frac{1}{n+1}} \tilde{\sigma}_{ij}\,(n,\theta)\,, \tag{35}$$

where I_n is an integration constant that depends on n and $\tilde{\sigma}_{ij}$ is a dimensionless function of n and θ. The values of these parameters are given for the cases of plane stress and plane strain conditions by Hutchinson (1968). It follows that the normal traction along the interface is given by

$$T_n = \sigma_0 \left[\frac{C^*}{\dot{\varepsilon}_0\, \sigma_0\, I_n\, r}\right]^{\frac{1}{n+1}} \tilde{\sigma}_\theta\,(n,0)\,, \tag{36}$$

In this analysis, we limit ourself to the case of $T_0 = \sigma_0$ and $m = n$. Therefore the opening separation rate for the simple model is evaluated from Eq. (8) as

$$\dot{\delta}_n = \dot{\delta}_0 \left[\frac{C^*}{\dot{\varepsilon}_0\, \sigma_0\, I_n\, r}\right]^{\frac{n}{n+1}} \tilde{\sigma}_\theta\,(n,0)^n\,. \tag{37}$$

The critical opening separation is determined by integrating the separation rate, in a similar way to in Eq. (8), as

$$\delta_n^{\mathrm{f}} = \int_0^{\infty} \dot{\delta}_n \cdot \frac{\mathrm{d}x_1}{\dot{a}} = \int_0^{r_{\mathrm{c}}} \dot{\delta}_n \cdot \frac{\mathrm{d}r}{\dot{a}} = (n+1)\, \frac{\dot{\delta}_0}{\dot{a}} \left[\frac{C^*}{\dot{\varepsilon}_0\, \sigma_0\, I_n}\right]^{\frac{n}{n+1}} r_{\mathrm{c}}^{\frac{1}{n+1}}\, \tilde{\sigma}_\theta\,(n,0)^n\,. \tag{38}$$

where $r = x_1$ at $\theta = 0$ and r_{c} is the size of the fracture zone which is very small in the case of stiff interface ($r_{\mathrm{c}} \to 0$). Rearrangement of Eq. (38) gives the dimensionless velocity as

$$\overset{\triangledown}{a} = (n+1)\, \frac{\bar{r}_{\mathrm{c}}^{\frac{1}{n+1}}}{\phi_0\, \bar{\delta}_n^{\mathrm{f}}} \left[\frac{f_n\,(n)}{I_n}\right]^{\frac{n}{n+1}} \tilde{\sigma}_\theta\,(n,0)^n\,, \tag{39}$$

where $\bar{r}_{\mathrm{c}} = r_{\mathrm{c}}/\lambda$. By comparing this equation with Eq. (30), the C_{s}-function for the case stiff interface becomes

$$C_{\mathrm{s}} = (n+1)\, \bar{r}_{\mathrm{c}}^{\frac{1}{n+1}} \left[\frac{2n}{n+1} \cdot \frac{1}{\phi_0\, I_n}\right]^{\frac{n}{n+1}} \tilde{\sigma}_\theta\,(n,0)^n\,. \tag{40}$$

For the case of $n = m = 9$ and $\theta = 0$, the integration constants are $I_9 \approx 3.025$ and $\tilde{\sigma}_\theta\,(9,0) \approx \tilde{\sigma}_\theta\,(13,0) \approx 1.2$ for the case of plane stress and $I_9 \approx 4.6$ and $\tilde{\sigma}_\theta\,(9,0) \approx \tilde{\sigma}_\theta\,(13,0) \approx 2.6$ for the case of plane strain (Hutchinson 1968). Thus, the C_{s}-functions for the cases of plane stress and plane strain conditions are $C_{\mathrm{s}} = 45.6 \cdot \bar{r}_{\mathrm{c}}^{0.1} \cdot \phi_0^{-0.9}$ and $C_{\mathrm{s}} = 7.1 \cdot 10^4 \cdot \bar{r}_{\mathrm{c}}^{0.1} \cdot \phi_0^{-0.9}$, respectively.

The other limit is when the interface is too compliant in comparison with the bulk material which can be regarded as rigid. Hence, in the case of an infinite DCB specimen, the equilibrium between the applied moment and the traction along the infinite damage zone suggests that the traction will tend to zero and there will be no crack propagation. on the other hand, when the specimen is finite a non zero traction along the finite damage zone. The deformation along the damage zone can directly be related to the angular deflection at the end of the beam. Thus, the separation at the crack tip is obtained as

$$\delta_n^{\mathrm{f}} = 2\,(L-a)\,\theta = 2\,W\,\theta, \tag{41}$$

where $W = L - a$ is the length of remaining ligament during steady state propagation. The opening displacement at the tip of the propagating crack is constant and equal to the critical value $\delta_n^{\mathrm{f}} = 0$, therefore $\dot{\delta}_n = 0$, and

$$\dot{a} = W\, \frac{\dot{\theta}}{\theta}. \tag{42}$$

Similarly, the separation at the crack tip can be written in this form

$$\dot{\delta}_n^{\mathrm{m}} = 2\, W \dot{\theta}. \tag{43}$$

The separation rate in the damage zone is given by

$$\dot{\delta}_n = \left[1 - \frac{x_1}{W}\right] \cdot \dot{\delta}_n^{\mathrm{m}}. \tag{44}$$

Now the balance by the internal and external work rates gives

$$2\, M\, \theta = \int_0^W T_n\, \dot{\delta}_n \cdot \mathrm{d}x_1 = \int_0^W \dot{\delta}_0\, T_0 \left(\frac{\dot{\delta}_n}{\dot{\delta}_0}\right)^{\frac{n+1}{n}} \cdot \mathrm{d}x_1. \tag{45}$$

Introducing Eq. (43) and the opening separation rate for the simple model in Eq. (8) we obtain the separation at the crack tip as

$$\dot{\delta}_n^{\mathrm{m}} = \dot{\delta}_0 \left[\frac{2n+1}{n}\, \frac{M}{\sigma_0\, W^2}\right]^n. \tag{46}$$

The crack velocity is determined from Eqs. (41), (42), (43) and (46) and using the definition of σ_0 in Eq. (20) as

$$\dot{a} = \frac{\dot{\delta}_0}{W^{2n-1}\, \delta_n^{\mathrm{f}}} \left[\frac{2}{\eta}\right]^n. \tag{47}$$

Scaling of Eq. (47) gives the dimensionless velocity as

$$\overset{\triangledown}{a} = \frac{1}{\phi_0\, \bar{W}^{2n-1}\, \bar{\delta}_n^{\mathrm{f}}} \left[\frac{2}{\eta}\right]^n \tag{48}$$

By comparing this equation with Eq. (30), the C_{s} function for the case compliant interface becomes

$$C_{\mathrm{s}} = \frac{1}{q_n^{\frac{n}{n+1}}\, \bar{W}^{2n-1}} \left[\frac{2}{\eta}\right]^n \phi_0^{-\frac{n}{n+1}}. \tag{49}$$

$\bar{W}$ is computed from the finite element analysis as the remaining ligament length when a crack reaches a steady state propagation. Hence, for the case of $n = m = 9$ and using the computationally obtained average value $\bar{W} \approx 0.8$, the C_s-functions for plane stress and plane strain conditions are $C_s = 10.5 \times 10^{-15} \cdot \phi_0^{-0.9}$ and $C_s = 38.3 \times 10^{-15} \cdot \phi_0^{-0.9}$, respectively.

Another limitation comes from the time scale of the crack propagation as mentioned in Sect. 2.1. C^* represents the near crack tip field when a crack propagates slowly. As the crack velocity increases elastic deformation becomes increasingly important in the vicinity of the crack tip and a zone in which both elastic and creep deformation determines the response becomes increasingly significant. If this zone becomes comparable in size to the damage zone, then C^* can no longer be used as a parameter for characterization of the near tip filed and damage growth process. Cocks and Julian (1991) studied this limit and proposed conditions for the dominance of C^*. They demonstrate that C^* controls crack growth provided the following condition is satisfied

$$\overset{\triangledown}{a} = f_n\,(n)^{\frac{1}{n+1}}\,\frac{Z\,(n)}{\sigma_0/E}\,\bar{r}_c^{\frac{2}{n+1}} \tag{50}$$

where E is Young's modulus and $Z\,(n) = (n-1)\;I_n{}^{\frac{n-1}{n+1}}$. Using this condition we derive a condition for C_s function by comparing Eq. (50) with Eq. (30) as

$$C_s \le \frac{2n}{n+1}\,f_n\,(n)^{\frac{1}{n+1}}\;Z\,(n)\;\frac{\bar{r}_c^{\frac{2}{n+1}}\,\bar{\delta}_n^{\mathrm{f}}}{\sigma_0/E}\;\phi_0^{\frac{1}{n+1}}. \tag{51}$$

This expression implies that for particular values of $\bar{\delta}_n^{\mathrm{f}}$ and σ_0/E there is a maximum velocity for which C^* is a valid measure. Thus, for the case of $n = m = 9$, the valid C_s-function for plane stress and plane strain conditions are $C_s \le 4.28 \cdot \dfrac{\bar{r}_c^{0.2}\,\bar{\delta}_n^{\mathrm{f}}}{\sigma_0/E} \cdot \phi_0^{0.1}$ and $C_s \le 6.0 \cdot \dfrac{\bar{r}_c^{0.2}\,\bar{\delta}_n^{\mathrm{f}}}{\sigma_0/E} \cdot \phi_0^{0.1}$, respectively.

Elasticity is only relevant in the computational models and this relationship can be used to assess whether the conditions employed in the FE models are consistent with the assumptions of the analytical model presented in Sect. 2. We need to be careful, however, when using this expression. It is derived from analyses in which damage development is assumed to not influence the near tip fields. As illustrated above, the size of the damage zone increases with decreasing ϕ_0 and for small ϕ_0 the near tip fields given by the classical continuum analysis are no longer valid. The relationship of Eq. (49) is therefore only valid in the limit of large ϕ_0 where the development of damage has limited effect on the crack tip fields. It is also important to emphasise here that although, the HRR field is no longer valid for small ϕ_0, C^* is still a valid parameter for characterizing crack growth.

In order to evaluate the proposed framework, C_s has been determined from (34) for ϕ_0 in the range $[10^{-10}, \times 10^5]$ and compared with the limiting results presented above. The rate sensitivity parameters are taken to be $n = m = 9$. Figure 12a, b show the relationship between C_s and ϕ_0 for plane stress and strain conditions, respectively.

Over the range of the data, the results can be fit using two separate power-law relations. Under plane stress conditions this relation is $C_s = 0.45\,\phi_0^{-0.06}$ over the range of values $\phi_0 \in [10^{-10}, 8 \times 10^{-2}]$ and $C_s = 0.09\,\phi_0^{-0.67}$ for the range $\phi_0 \in [8 \times 10^{-2}, 10^3]$, see the dashed lines in Fig. 12a. The transition between the power law relations occurs over the range $10^{-4} \le \phi_0 \le 10^0$. For a given value of ϕ_0, C_s lies between the two limiting values. The power-law fit for high values of ϕ_0 is slightly shallower than that for the stiff limit described above, indicating that response tends to this limit for values of ϕ_0 in excess of 10^6. In this limit the rate of deformation in the damage zone becomes very small compared to that in the surrounding matrix, which determines the stress distribution ahead of the crack tip and therefore the rate of growth of damage. There is no evidence of the data merging to the limiting result for low values of ϕ_0, but the values of ϕ_0 required to reach this limit are much lower than values we would expect from physical arguments (in this limit the material length scale is significantly greater that the geometric length scale—in practice we would expect any characteristic material length scale to be less than the geometric length scale for the cracked body, i.e. we would expect ϕ_0 to be greater than 1). The power-law range for ϕ_0 greater than 8×10^{-2} is therefore more representative of the physical behaviour of engineering components, so we concentrate on the relation for this regime here. Substituting this relationship into Eq. (30) gives the dimensionless velocity

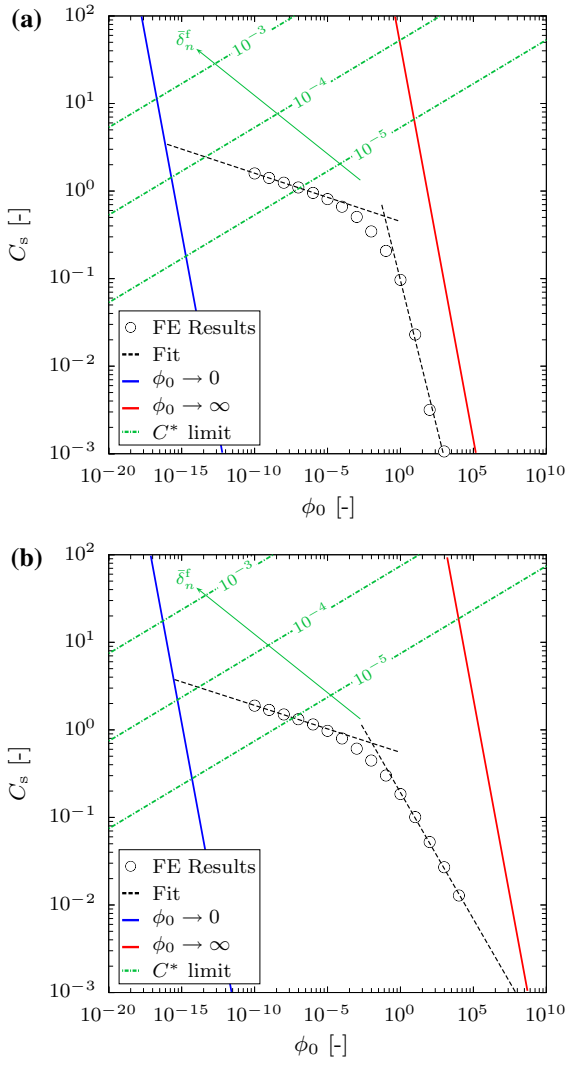

Fig. 12 The relation between C_s-function and ϕ_0 parameter and the physical limits in the case of $n = m = 9$: **a** plane stress conditions; **b** plane strain conditions. The *red* and *blue lines* represent the compliant and stiff limits, respectively, the *green dash-dot lines* represent the C^* validity limit for different dimensionless separation at failure $\bar{\delta}_n^f$, and the *dashed lines* show the power law fit

$$\overset{\triangledown}{a} = 1.18 \times 10^{-2} \cdot \frac{\phi_0^{-0.77}}{\bar{\delta}_n^f}. \tag{52}$$

or into Eq. (31), the velocity in terms of C^*:

$$\begin{aligned} \dot{a} &= 9.0 \times 10^{-2} \cdot \frac{A^{0.77}\,\lambda^{0.33}}{\delta_n^f\,B^{0.67}} \left[0.56\,C^*\right]^{0.9} \\ &= 1.19 \times 10^{-2} \cdot \frac{A^{1.32}\,B^{0.23}\,\lambda^{1.23}\,\sigma_0^9}{\delta_n^f}. \end{aligned} \tag{53}$$

where we have substituted for C^* using Eq. (21) to provide a relationship in terms of the reference stress σ_0. Figure 12a also shows a series of lines below which elastic effects can be ignored for $\sigma_0/E = 8 \times 10^{-6}$ (as used in the computations) and different values of critical crack tip opening displacement, i.e. below which inequality (51) is satisfied. As noted earlier this relationship is only valid for large values of ϕ_0 (say greater than 8×10^{-2}). In this regime the computational results lie below this series of lines, indicating that the theoretical structure presented in Sect. 4 provides a valid framework for modelling the crack growth behavior.

We can repeat the analysis for plane strain conditions, see Fig. 12b. In the case of plane strain we again find that the results can be fit using two power-law relationships: $C_s = 0.55\,\phi_0^{-0.05}$ over the range of values $\phi_0 \in [10^{-10}, 10^{-2}]$ and $C_s = 0.19\,\phi_0^{-0.29}$ for the range $\phi_0 \in [10^{-2}, 10^{4}]$, see the dashed lines in Fig. 12b. Further, the transition between the power law relations takes place in the range $10^{-4} \le \phi_0 \le 10^{0}$. The latter relation gives a dimensionless crack growth rate of

$$\overset{\triangledown}{a} = 2.5 \times 10^{-2} \cdot \frac{\phi_0^{-0.39}}{\bar{\delta}_n^f}. \tag{54}$$

The comparison between the FE results and the physical limits is also shown in Fig. 12b, which are again bounded by the physical limits of Eqs. (40) and (49), with the results asymptoting to Eq. (40) at large values of ϕ_0. The large limit ϕ_0 gives a faster crack growth rate in plane strain than plane stress (i.e. C_s is larger for a given value of ϕ_0) due to the higher stress levels ahead of a plane strain crack. The difference in slope between this limit and the computational results is greater than that observed for plane stress, but the value of ϕ_0 where the two curves meet is about two orders of magnitude higher. As for plane stress, the results lie in a regime where elastic effects can be ignored.

4.4 The effect of damage model

In order to investigate the effect of the detailed form of the damage zone model on the crack growth response, $\hat{C}_k$ has been determined for each of the different damage zone models described in Sect. 2. The parameters employed for these models are $m = 9$, $\delta_n^f = 0.02$ mm, $\beta = 1.0$, $h_0 = 0.02$ mm, $f_0 = 0.01$ and $f_c = 0.5$. It should be noted that δ_n is kept constant for all models.

Further, we choosed $g_0 = 2.23$ and $\beta = 1.0$ such that all models yield the same rupture time t_f under a prescribed constant stress. (In "Appendix B" we demonstrate that under a given stress and for prescribed values of $\dot{\delta}_0$ and δ_n^f the time to failure is proportional to a dimensionless quantity $\tilde{I}_k$, see Eq. (B.6). We choose the values β and g_0 in the exponential Kachanov and micromechanical models such that $\tilde{I}_k$, and therefore the time to failure, is the same for all the models). In the studies of crack growth, the physical length scale of the cracked body $\lambda = H/2$ is used and the matrix rate sensitivity parameter is taken to be $n = 9$, as before. Here, we limit our consideration to plane stress conditions, but similar results can be obtained under plane strain. $\hat{C}_k$ is determined using the same procedure as described above, by comparing the computed steady state crack growth rate with Eq. (34). As before, we can determine analytical relationships for the response in the limits of small and large ϕ_0. In Sect. 4.3 we found that the analytical model in the limit as $\phi_0 \to 0$ does not provide a meaningful bound to the results and we do therefore do not present results in this limit for the remaining damage zone models described in Sect. 2. The analytical results for these models in the limit $\phi_0 \to \infty$ are presented in "Appendix C".

Rather than express $\hat{C}_k$ as a function of ϕ_0 it proves instructive to express it as a function of $\hat{C}_k$ (which is a function of ϕ_0) for each of the models. Figure 13 shows the relationship between $\hat{C}_k$ and $\hat{C}_s$. The results show that these relations are nonlinear. However, for each model there is *point-wise* a linear relationship between these two functions with

$$\hat{C}_k = \mu_k \hat{C}_s. \tag{55}$$

where μ_k is a parameter that depends on the damage model used. The effect of damage is to soften the constitutive response, effectively increasing the effective separation rate across the damage zone for a given traction T_n, which results in a lower effective value of ϕ_0 and therefore an increase of the crack growth rate. Therefore μ_k is larger than 1.0 for a given value of δ_n^f. Values μ_k are given in "Appendix C" for the three models: $\mu_{kl} = \mu_{ke} = \mu_m = 10$. Substituting these values of μ_k into Eq. (55) give the straight lines plotted in Fig. 13, which also shows the computational results.

The computational results approach the analytical results for small values of $\hat{C}_s$, i.e. large values of ϕ_0, see Fig. 13, which corresponds to the limit where we would expect the analytical result to apply. As is increased gradually reduces for all the models and then asymptotes to a value $\mu_{kl} = \mu_{ke} = \mu_m = 1.8$. As $\hat{C}_s$ increases deformation in the damage zone becomes constrained and the stress relaxes more for a damaged material for a given value of ϕ_0 compared to a material that does not damage. Therefore, the elevation of the crack growth rate is less. In the limit that deformation is completely constrained [corresponding to the situation considered by Cocks and Ashby (1981)] the crack velocity is independent of the details of the model and only depends on the critical opening displacement δ_n^f; thus in this limit we would expect μ_k to equal 1 for all the models considered here. This represents a physical lower bound to μ_k, which is not reached for any of the models with the results appearing to asymptote to a higher limiting value over the range of conditions considered in the computations.

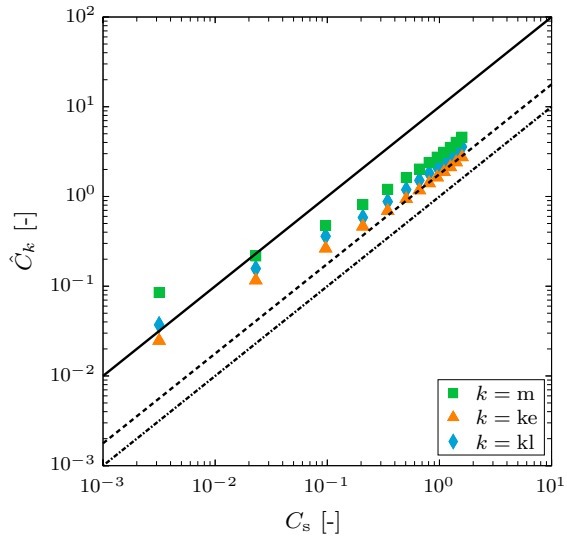

Fig. 13 The relation between $\hat{C}_k$ and C_s (which is a function of ϕ_0 parameter—see Fig. 12a for the different models under plane stress conditions. The *solid line* represent the response given by the model presented in "Appendix C". The *dashed line* represent the apparent asymptotic behaviour. The *chained line* corresponding to $\mu_k = 1$ represents a strict lower bound to the data

4.5 Comparison with experimental data

The main objective of this paper is to identify simple constitutive models for the damaging process ahead of a crack tip in a creeping material and to identify

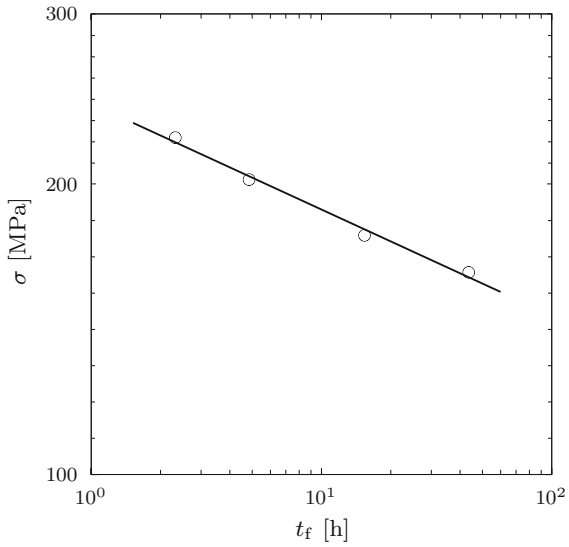

Fig. 14 Comparison between uniaxial creep rupture data for 2.25 Cr Mo steel at 538 °C and the interface damage model in (B.6). '○' represents the experimental data and the *black line* indicates the model predictions

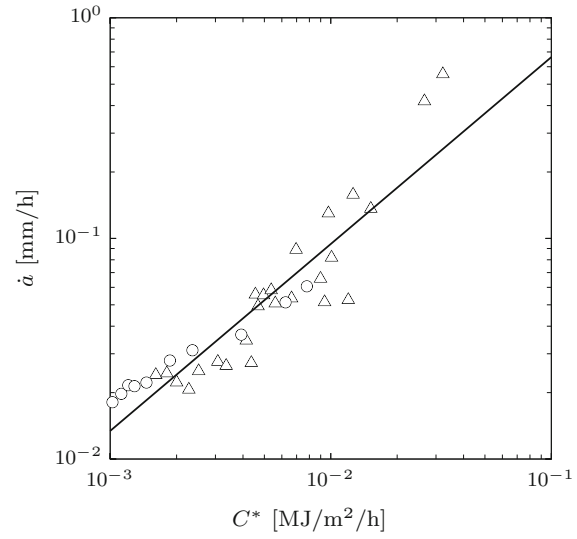

Fig. 15 Comparison between experimental creep crack growth data for 2.25 Cr Mo steel at 538 °C and the proposed framework. '○' and '△' represents the exprimental data for $B_n = 6$ mm and $B_n = 10$ mm, respectively, and $B = 25$ mm. The *black line* indicates the framework predictions for the different damage models

a simple structural configuration which can be analysed rigorously to provide new insights into the relationship between damage models and the crack growth process, including the role of different characteristic material and geometric length scales. As a result, the simple geometry and loading conditions considered are not representative of laboratory test components. Nonetheless, it proves instructive to explore how the models presented here can be calibrated against available experimental data, to determine the characteristic material and geometric length scales in these experiments and explore where this data lies with respect to the general trends identified in Figs. 14 and 15.

In this section, we consider the low alloy steel (2.25 Cr Mo steel at 538 °C) investigated by Nikbin et al. (1983). They provide data for creep deformation, creep rupture as well as creep crack growth generated using compact tension (CT) specimens, see Figs. 14 and 15. Consider the creep crack law of Eq. (31), together with the definition of ϕ_0 in Eq. (32) or following Eq. (26). In order to determine the crack growth rate we need to determine the characteristic length λ for the cracked geometry and the material parameters n, m, δ_n^{f} and $\dot{\varepsilon}_0$, $\dot{\delta}_0$ (at a reference stress σ_0) or equivalently the material parameters A and B. The steady creep response under a constant uniaxial stress σ is given by Nikbin et al. (1983) at 538 °C:

$$\dot{\varepsilon} = \dot{\varepsilon}_0 \left(\frac{\sigma}{\sigma_0}\right)^n = B\,\sigma^n, \tag{56}$$

where $n = 9$ and $B = 10^{-23}$ MPa^{-9} h^{-1}.

In the remainder of the fitting process described in detail here we limit our consideration to the linear Kachanov model. Parallel procedures can be undertaken for the other damage models described in this paper. In determining the material parameters we assume that the damage zone model can also be used to describe damage development on grain boundaries in a uniaxial test. We further assume that damage grows primarily on boundaries normal to the direction of the applied stress. Integrating the damage growth rate equation between the limits $\omega = 0$ at time $t = 0$ and $\omega = 1$ at failure, i.e. when $t = t_{\mathrm{f}}$, then gives (see "Appendix B")

$$t_{\mathrm{f}} \cdot \sigma^m = \frac{\sigma_0^m}{m+1}\left(\frac{\delta_n^{\mathrm{f}}}{\dot{\delta}_0}\right) = \frac{1}{m+1}\left(\frac{\delta_n^{\mathrm{f}}}{A}\right) = D. \tag{57}$$

Creep rupture data given by Nikbin et al. (1983) is plotted in Fig. 14, which gives $m = 9$, $D = 2.7 \times 10^{22}$ MPa$^9 \cdot$ h, thus providing a relationship between two of the material parameters

$$\delta_n^{\mathrm{f}} = 2.7 \times 10^{23}\, A \ [\mathrm{mm}]. \tag{58}$$

where A is measured in units of $\mathrm{mm}/(\mathrm{MPa}^9 \cdot \mathrm{h})$.

In the second step, we determine another relationship between δ_n^{f} and A from fitting the creep crack growth data ($\dot{a}$ vs C^*) to the model in Eq. (31). This combined with Eq. (58) provides two equations in terms of the two unknowns δ_n^{f} and A. To do this, we must represent Eq. (31) in terms of the fitting parameters δ_n^{f} and A. To do this we also need to determine the geometric length scale for the compact tension specimen employed in the crack growth studies. This requires the identification of an expression for C^*. Here we employ an expression employed in the UK R5 assessment procedure (Ainsworth et al. 1987), which is equivalent in form to the relationship derived for the double cantilever beam (Eq. 21), i.e.

$$C^* = \dot{\varepsilon}_0\, \sigma_0\, \lambda, \tag{59}$$

where $\dot{\varepsilon}_0$ is the uniaxial strain rate at a reference stress σ_0 (Ainsworth et al. 1987). The reference stress is defined by

$$\sigma_0 = \frac{P}{P_{\mathrm{L}}}\, \sigma_{\mathrm{y}}, \tag{60}$$

where P_{L} is the limit load for a perfectly plastic material of yield strength σ_{y} and P is the applied load. The characteristic length scale λ for a component is defined by $\lambda = K_{\mathrm{I}}^2/\sigma_0^2$ where K_{I} is the stress intensity factor for the specimen at the applied load P. For a compact tension specimen the limit load for the case of plane stress (Miller and Ainsworth 1989) is given by

$$P_{\mathrm{L}} = \sigma_{\mathrm{y}} \cdot W \cdot \underbrace{\left\{ \left[(1+\gamma) \cdot \left(1 + \gamma \left(\frac{a}{W} \right)^2 \right) \right]^{\frac{1}{2}} - \left(1 + \frac{a}{W} \right) \right\}}_{\Upsilon_{\mathrm{L}}}, \tag{61}$$

where Υ_{L} is a shape function, $\gamma = 1.155$, a is the crack length and W is the width of the specimen. The mode I stress intensity factor is given by

$$K_{\mathrm{I}} = \frac{P}{W^{\frac{1}{2}}} \cdot \Upsilon_{\mathrm{K}}, \tag{62}$$

where the shape function Υ_{K} is given by

$$\Upsilon_{\mathrm{K}} = \frac{2 + \frac{a}{W}}{\left(1 - \frac{a}{W}\right)^{\frac{3}{2}}} \cdot \left[0.886 + 4.64 \cdot \left(\frac{a}{W} \right) - 13.32 \cdot \left(\frac{a}{W} \right)^2 + 14.72 \cdot \left(\frac{a}{W} \right)^3 - 5.60 \cdot \left(\frac{a}{W} \right)^4 \right]. \tag{63}$$

Hence, the characteristic length scale is given by

$$\frac{\lambda}{W} = (\Upsilon_{\mathrm{L}} \cdot \Upsilon_{\mathrm{K}})^2. \tag{64}$$

Miller and Ainsworth (1989) compared the predictions of Eq. (59) with detailed finite element calculations and suggested a modification to this expression to provide a better agreement with the computational results:

$$C^* = \dot{\varepsilon}_0\, \sigma_0\, \lambda\, F_{\mathrm{p}}^{n+1}. \tag{65}$$

where F_{p} is a dimensionless parameter which is in the range 0.92 to 0.96 for $n = 9$ and a/W in the range 0.25 to 0.5. Here we use an average value of 0.94. Equation (65) effectively reduces the reference stress by a factor F_{p}, but does not change the expression for the characteristic length.

For the CT specimen tested by Nikbin et al. (1983) $W = 50$ mm and the initial crack length was $a_0 = 12.5$ mm. The crack growth rate is plotted as a function of C^* in Fig. 15, which covers a 2 orders of magnitude increase in C^* over the period of stable crack growth. From Eq. (64) we find that a two orders of magnitude increase in C^* corresponds to an increase of crack length from a/W to 0.25 to 0.4. From Eq. (64) we find that this corresponds to a change of characteristic length from $\lambda/W = 1.3$ to 1.0. In our evaluation of the data we take an average of these values for the characteristic length, i.e. $\lambda/W = 1.15$. In order to proceed we need to determine which expressions to use for $\hat{C}_k$ in Eq. (31), i.e. which regions of Figs. 12a and 13 the data lies in. From the creep deformation and creep rupture data presented earlier we find $\dot{\varepsilon}_0 = 1.24 \times 10^{-24}\, \sigma_0^9$ 1/h and $\phi_0 = 2.17 \times 10^2/\delta_n^{\mathrm{f}}$ [defined after Eq. (26)], which suggests that for typical expected critical opening displacements in metals ($\delta_n^{\mathrm{f}} \in [10^{-10} - 10^{-5}]$ m, i.e. of the order of the mean cavity spacing) $\phi_0 > 1.0$. Therefore, we use the power-law relation for $\phi_0 > 1.0$ which is $\hat{C}_{\mathrm{kl}} = 0.40 \cdot \phi_0^{-0.494}$. In this regime, Eq. (31) can be written in the form

Table 1 The damage models parameters

Interface model, k	m [−]	A [mm/(MPa^9 h)]‡	δ_n^{f} [μm]†	β [−]	h_0 [μm]	f_0 [−]	f_{c} [−]
kl	9	8.84×10^{-27}	1.10×10^2	–	–	–	–
ke	9	4.15×10^{-25}	2.35×10	–	–	–	–
m	9	1.71×10^{-26}	4.56×10	–	1.88	0.00032	0.71

† δ_n^{f} is calculated using Eq. (13) for the micromechanical model
‡ Note, σ_0 changes during the duration of a test, causing $\dot{\varepsilon}_0$ and $\dot{\delta}_0$ to also change. At a given instant σ_0 can be determined from Eq. (60), multiplied by $F_{\mathrm{p}} = 0.94$, to take into account the correction of Miller and Ainsworth (1989)

$$\dot{a} = 1.18 \times 10^{-5} \cdot \frac{C^{*0.9}}{\delta_n^{\mathrm{f}\,0.41}}, \tag{66}$$

where $\dot{a}$ is in mm/h, δ_n^{f} is in mm and C^* is in MJ/mm2/h. Fitting this expression to the data of Fig. 15 gives the critical separation δ_n^{f}. The rate parameter B can then be determined from Eq. (58). We can employ the same fitting procedure for the exponential Kachanov and micromechanical models. In these models additional parameters are required, i.e. β for the exponential Kachanov model and h_0, f_0 and f_{c} for the micromechanical model. For $\phi_0 > 1.0$, $\hat{C}_{\mathrm{ke}} = 0.30 \cdot \phi_0^{-0.515}$ and $\hat{C}_{\mathrm{m}} = 0.49 \cdot \phi_0^{-0.373}$ for the exponential Kachanov and micromechanical models. Using a nonlinear least squares method, the crack growth rate in Eq. (66) is then fitted to the creep crack growth data. Figure 15 shows the comparison between experimental creep crack growth data and the framework predictions for different damage models (they all lie on the same straight line and yield comparable goodness of fit). The fitting parameters are shown in Table 1 for the different models. The parameters indicate that the material data falls in regime close to the stiff limit, i.e. $\phi_0 \in [10^3 - 10^4]$. Further, the failure separation falls within the physical regime, i.e.

In the above analysis we noted that the characteristic length scale only changes by a small amount during the course of an experiment (i.e. by less than 13% from the mean value), while C^* changes by over 2 orders of magnitude, thus the effect of C^* swamps that due to λ and we could assume a constant value of λ when fitting the data. We need to be careful, however when using the developed model to assess the growth of defects in high temperature components. In general, any defects of interest will be much smaller than that employed in laboratory experiments, such as the CT specimens considered here. Conventional models of creep crack growth determined from experimental data do not include the effect of λ on the crack growth rate, other than how it affects C^* (i.e. experimental laws generally assume that $\dot{a} \propto C^{*q}$, where $q < 1$). This has two major consequences. Firstly, the models developed from the data give a crack growth rate that is proportional to λ^p, where p is of the order of 0.5. Thus as the crack size is reduced the crack growth rate reduces compared with that determined from the laboratory data for the same value of C^*. Thus use of laboratory data overestimates the crack growth rate. Secondly, as λ is reduced ϕ_0 also reduces and damage growth ahead of a crack tip becomes more constrained, with the loading condition moving to the left on Fig. 12 and towards the top right corner on Fig. 13. This can result in a transition to the low ϕ_0 regime where now $p \approx 1.0$. The crack growth rate is now more sensitive to the size of the defect and the laboratory data provides an even more significant overestimation of the crack growth rate.

5 Concluding remarks

In this study, a combined theoretical and computational study for crack growth under steady state conditions is presented. A theoretical framework is introduced in which the constitutive behaviour of the bulk material is described by power-law creep. A new class of damage zone models is proposed to model the fracture process such that the constitutive relation is described by a traction-separation rate law. Further, three different damage zone models are investigated: a simple critical displacement model; empirical Kachanov damage type models; and a micromechanical model. The path independence of the C^*-integral is used to relate the far field loading to the damage growth process along a narrow zone directly ahead of the growing crack tip. A double cantilever beam specimen (DCB) subjected to constant pure bending moment is studied and analytical models are developed for pure mode-I steady-state

crack growth. Further, using dimensional analysis the dimensionless functions C_s and $\hat{C}_k$ are derived which account for the detailed form of the model on the crack growth process. A computational framework is then implemented using the Finite Element method and the analytical models are calibrated against detailed Finite Element simulations, allowing the C_s and $\hat{C}_k$ functions to be determined for different combinations of dimensionless parameters. The $\hat{C}_k$ function depends on the ratio of geometric to material length scales for the problem, ϕ_0, and the rate sensitivity exponents n and m. The C_s-function is found to take two different power law forms over a wide range of values of ϕ_0. Two simple models are presented by consider the response as $\phi_0 \to 0$ and $\phi_0 \to \infty$, which bound the computational results. The crack velocity asymptotes to the $\phi_0 \to \infty$ limit as ϕ_0 increases. Incorporation of the effect of damage into the constitutive response for the damage zone, results in a more substantial relaxation of stress ahead of the crack tip and a faster crack growth rate for a given value of ϕ_0 and a delay in the asymptote to the $\phi_0 \to \infty$ limit. Comparison with experimental data for a 2.25 Cr Mo steel at 538 °C shows that the different damage models are capable of fitting creep crack growth data using physically reasonable parameters.

In this paper we have used simple material models for the matrix and damage zone response to analyses crack growth in a simple geometry. Nonetheless, the calculations provide a useful framework for evaluating the effect of different damaging processes on crack growth and evaluating data for more complex laboratory specimens.

Acknowledgements The authors are grateful to EPSRC for supporting the research presented in this paper under Grant number EP/K007866/1.

A Appendix: Finite Element formulation of the interface element

The interface damage models in Sect. 2.3 have been implemented into the Finite Element method using cohesive element approach. For the implementation purposes, the traction-separation rate law is assumed to be determined by elastic and creep responses, i.e. the total separation is decomposed into elastic and creep contributions. Therefore, the total separation rates are written as

$$\dot{\delta}_i = \dot{\delta}_i^{\mathrm{el}} + \dot{\delta}_i^{\mathrm{cr}} \tag{A.1}$$

where $i \in [t, n]$ and $\dot{\delta}_i^{\mathrm{el}}$ and $\dot{\delta}_i^{\mathrm{cr}}$ are the elastic and creep separation rates, respectively. Additionally, this study is limited to pure mode I loading, the creep behaviour is only considered in the normal direction and the response of the tangential direction is taken to be purely elastic. The traction-separation rate laws for the tangential and normal directions are respectively defined as

$$\dot{\delta}_i = \dot{\delta}_n^{\mathrm{el}} = \frac{\dot{T}_t}{K_t}, \tag{A.2}$$

and

$$\dot{\delta}_n = \dot{\delta}_n^{\mathrm{el}} + \dot{\delta}_n^{\mathrm{cr}} = \frac{\dot{T}_n}{K_n} + \dot{\delta}_0 \left(\frac{T_n}{d_k\, T_0} \right)^m. \tag{A.3}$$

where K_t and K_n are the elastic stiffness parameters in the tangential and normal directions, respectively. The damage function d_k depends on the normal creep separation δ_n^{cr}.

The surface-like cohesive formulation is adopted in this work (e.g. see Willam et al. 1989; Ortiz and Suresh 1993; Xu and Needleman 1993; Ortiz and Pandolfi 1999). In this formulation, a cohesive element consists of two surface elements which coincide in the reference configuration. The upper and lower surface elements are denoted S^+ and S^-, respectively, and the constitutive behaviour of the cohesive element is defined in a middle surface $\bar{S}$. A 4-node two-dimensional linear element is used in this study. The middle surface is defined by the two points 1–2 which are the mid-points between nodes 1^-–2^- and 1^+–2^+ in the lower and upper elements, respectively, see Fig. 16. Hence, the middle surface is then defined by the interpolation

$$\mathbf{x} = \sum_{a=1}^{2} N_a\, \bar{\mathbf{x}}_a, \tag{A.4}$$

where $\bar{\mathbf{x}}_a$ is the current coordinates vector of the middle surface which is related to the current nodal coordinates of the upper and lower surface elements $\mathbf{x}_a^+$ and $\mathbf{x}_a^-$, respectively, by

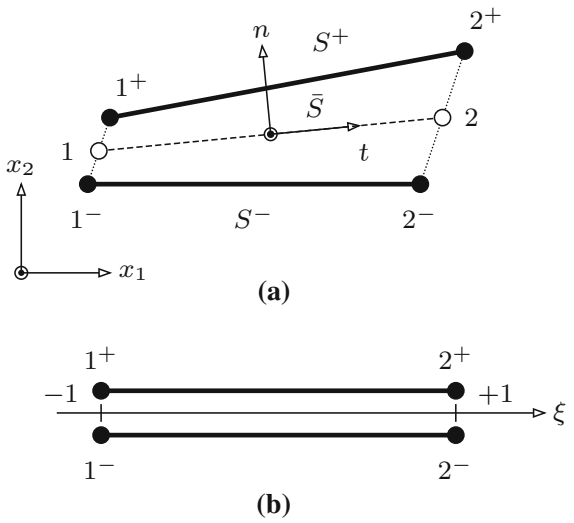

Fig. 16 Geometry of an interface element: **a** the physical domain and **b** the parent domain. The definition of the surfaces S^-, S^+ and $\bar{S}$ that coincide in the reference configuration

$$\bar{\mathbf{x}}_a = \frac{1}{2}\left(\mathbf{x}_a^+ + \mathbf{x}_a^-\right). \tag{A.5}$$

The standard shape functions, $N_a = N_a^- = N_a^+$, are defined in the local coordinates, $\xi \in [-1, 1]$, as

$$N_1 = \frac{1}{2}(1-\xi), \tag{A.6}$$

$$N_2 = \frac{1}{2}(1+\xi). \tag{A.7}$$

Similarly, the global displacement jump across the cohesive element, $\bar{\mathbf{u}}$, is defined in points 1 and 2 as

$$\mathbf{u} = \sum_{a=1}^{2} N_a\, \bar{\mathbf{u}}_a, \tag{A.8}$$

where $\bar{\mathbf{u}}_a$ is the displacement jumps of the middle surface which is related to the nodal displacement by

$$\bar{\mathbf{u}}_a = \mathbf{u}_a^+ - \mathbf{u}_a^-. \tag{A.9}$$

The finite element formulation is developed from principle of virtual work where the nodal forces and the stiffness matrix are computed. Hence, the principle of virtual work for the interface zone is defined as

$$\delta\Pi_{\text{int}} = \int_{\Gamma_{\text{int}}} \mathbf{T}\,\delta\boldsymbol{\delta}\cdot \mathrm{d}S, \tag{A.10}$$

where Γ_{int} is the interface surface, $\mathbf{T}$ is the traction vector across the interface and $\delta\boldsymbol{\delta}$ is the virtual separation that are defined in the local coordinate system. The internal nodal force across the interface surface is determined from the tractions and by substitution of the finite element interpolation into Eq. (A.10) as

$$\mathbf{f}_{\text{int}}^{\pm a} = \int_{\Gamma_{\text{int}}} \mathbf{T}\, N_a \cdot \mathrm{d}S. \tag{A.11}$$

The consistent tangent stiffness matrix is determined from the linearization of Eq. (A.11), with the result

$$\mathbf{K}_{\text{int}}^{\pm} = \frac{\partial \mathbf{f}_{\text{int}}^{\pm a}}{\partial \boldsymbol{\delta}_b} = \int_{\Gamma_{\text{int}}} N_a \frac{\partial \mathbf{T}}{\partial \boldsymbol{\delta}}\, N_b \cdot \mathrm{d}S. \tag{A.12}$$

It should be noted that the nodal forces and the consistent tangent matrix are defined in the local coordinate system (t, n) and a transformation to the global system $(1, 2)$ is needed before assembling to the finite element equations. This transformation includes mapping from the local to the global coordinates and relating the local to the global nodal numbering.

A.1 The cohesive element traction

The tractions are determined using the incremental forms of the total separation rates in Eqs. (A.2) and (A.3). Hence, a set of equations is obtained from these incremental form at the $i+1$th increment as

$$H_t = \Delta\delta_t - \frac{\Delta T_t}{K_t} = 0, \tag{A.13}$$

$$H_n = \Delta\delta_n - \frac{\Delta T_n}{K_n} + \Delta t\, \dot{\delta}_0 \left(\frac{T_n^i + \Theta \Delta T_n}{d_k\, T_0}\right)^m = 0, \tag{A.14}$$

where Δt is the time increment, T_i^n is the normal traction at the start of the increment and Θ is integration parameter $(1 \geq \Theta \geq 0)$.

In order to solve these equations, we use encapsulate the equations in a vector $\mathbf{H} = [H_t \quad H_n]^{\mathrm{T}}$ and define the unknown vector $\Delta\mathbf{T} = [\Delta T_t \quad \Delta T_n]^{\mathrm{T}}$. Using Newton-Raphson algorithm, the following linearized form of these equations is iteratively solved for the traction increment until a convergence condition is achieved

$$\mathbf{H}\left(\Delta\mathbf{T}+\delta\Delta\mathbf{T}\right)=\mathbf{H}\left(\Delta\mathbf{T}\right)+\underbrace{\frac{\partial\mathbf{H}}{\partial\Delta\mathbf{T}}}_{\mathbf{J}}\delta\Delta\mathbf{T}=\mathbf{0} \quad \text{(A.15)}$$

where $\mathbf{0}$ is a zeros vector (2×1) and the Jacobian $\mathbf{J}$ is defined as

$$\mathbf{J}=\begin{bmatrix}\dfrac{\partial H_t}{\partial\Delta T_t} & \dfrac{\partial H_t}{\partial\Delta T_t}\\ \dfrac{\partial H_n}{\partial\Delta T_t} & \dfrac{\partial H_n}{\partial\Delta T_n}\end{bmatrix}, \quad \text{(A.16)}$$

where

$$\frac{\partial H_t}{\partial\Delta T_t}=-\frac{1}{K_t}, \quad \text{(A.17)}$$

$$\frac{\partial H_t}{\partial\Delta T_n}=0, \quad \text{(A.18)}$$

$$\frac{\partial H_n}{\partial\Delta T_t}=0, \quad \text{(A.19)}$$

$$\frac{\partial H_n}{\partial\Delta T_n}=-\frac{1}{K_n}-\Delta t\,\frac{\dot{\delta}_0}{d_k\,T_0}\,\Theta\,(m-1)\times\left[\frac{T_n^i+\Theta\Delta T_n}{d_k\,T_0}\right]^{m-1}. \quad \text{(A.20)}$$

A.2 The cohesive zone Jacobian

The definition of the cohesive zone Jacobian in Eq. (A.12) yields interface tangent modulus as

$$\mathbb{C}=\frac{\partial\Delta\mathbf{T}}{\partial\Delta\boldsymbol{\delta}}=\begin{bmatrix}\dfrac{\partial\Delta T_t}{\partial\Delta\delta_t} & \dfrac{\partial\Delta T_t}{\partial\Delta\delta_t}\\ \dfrac{\partial\Delta T_n}{\partial\Delta\delta_t} & \dfrac{\partial\Delta T_n}{\partial\Delta\delta_n}\end{bmatrix}, \quad \text{(A.21)}$$

The elements of the tangent modulus can be determined from the variations of the incremental forms in Eqs. (A.14). The variation of H_i is given by

$$\delta H_i=\frac{\partial H_i}{\partial\Delta\delta_t}\cdot\delta\Delta\delta_t+\frac{\partial H_i}{\partial\Delta\delta_n}\cdot\delta\Delta\delta_n=0 \quad \text{(A.22)}$$

where the variations of the separation increments $\delta\Delta\delta_t$ and $\delta\Delta\delta_n$ can be chosen arbitrarily yielding that $\partial H_i/\partial\Delta\delta_t=0$ and $\partial H_i/\partial\Delta\delta_n=0$. Hence, the variations of Eqs. (A.14) gives

$$\frac{\partial H_t}{\partial\Delta T_t}=\frac{1}{K_t}, \quad \text{(A.23)}$$

$$\frac{\partial H_t}{\partial\Delta T_n}=0, \quad \text{(A.24)}$$

$$\frac{\partial H_n}{\partial\Delta T_t}=0, \quad \text{(A.25)}$$

$$\frac{\partial H_n}{\partial\Delta T_n}=\frac{1+\Delta t\,\dfrac{\dot{\delta}_0}{d_k\,T_0}\,\Theta\,(m-1)\left[\dfrac{T_n^i+\Theta\Delta T_n}{d_k\,T_0}\right]^m\dfrac{\partial d_k}{\partial\Delta\delta_n}}{\dfrac{1}{K_n}+\Delta t\,\dfrac{\dot{\delta}_0}{d_k\,T_0}\,\Theta\,(m-1)\left[\dfrac{T_n^i+\Theta\Delta T_n}{d_k\,T_0}\right]^{m-1}}. \quad \text{(A.26)}$$

In the case of high values of K_n the derivative of the damage function for good approximation can be taken as $\partial d_k/\partial\Delta\delta_n\approx\partial d_k/\partial\Delta\delta_n^{\mathrm{cr}}$.

B Appendix: Prediction of interface damage

In this appendix we will develop relations for interface damage. Consider a constant uniaxial stress state given by $T_n=\sigma$ such that damage is accumlated from an initial value to complete failure in a time t_{f} (rupture life), i.e. $\omega\in[0,1]$ and $f\in[f_0,f_{\mathrm{c}}]$. The rupture life is obtained by integration of the relation between the damage parameter and the traction which is derived from the relationship between $\dot{\delta}_n$ and T_n and the damage evolution law. A general form of the relationship between $\dot{\delta}_n$ and T_n is expressed as

$$\dot{\delta}_n=\dot{\delta}_0\left(\frac{T_n}{d_k\,T_0}\right)^m, \quad \text{(B.1)}$$

where the function d_k is given in Eq. (23) for the different interface models. Rearranging and integrating (B.1) gives

$$\int_{\delta_n^{\mathrm{c}}}^{\delta_n^{\mathrm{f}}}{d_k}^m\cdot\mathrm{d}\delta_n=\dot{\delta}_0\left(\frac{\sigma_n}{\sigma_0}\right)^m\cdot\int_0^{t_{\mathrm{f}}}\mathrm{d}t. \quad \text{(B.2)}$$

where δ_n^{c} is the opening at the initiation of damage and δ_n^{f} is the critical opening. We assume $\delta_n^{\mathrm{c}}=0$ for simplicity. The left-hand side of this equation, $I_k=\int{d_k}^m\cdot\mathrm{d}\delta_n$, is evaluated by replacing the separation increment $\mathrm{d}\delta_n$ with the damage parameter increment (i.e. $\mathrm{d}\omega$ or $\mathrm{d}f$) using the evolution laws in Eqs. (11), (12) and (15). Thus, for the case of Kachanov damage type models

$$I_{\mathrm{kl}} = \int_0^{\delta_n^{\mathrm{f}}} {d_{\mathrm{kl}}}^m \cdot \mathrm{d}\delta_n = \int_0^1 (1-\omega)^m \ \delta_n^{\mathrm{f}} \cdot \mathrm{d}\omega = \frac{\delta_n^{\mathrm{f}}}{m+1}, \quad \text{(B.3)}$$

and

$$I_{\mathrm{kl}} = \int_0^{\delta_n^{\mathrm{f}}} {d_{\mathrm{ke}}}^m \cdot \mathrm{d}\delta_n = \int_0^1 (1-\omega)^m \ \frac{\delta_n^{\mathrm{f}}}{\beta} \cdot \mathrm{d}\omega = \frac{\delta_n^{\mathrm{f}}}{\beta\,(m+1)}, \quad \text{(B.4)}$$

for the exponential damage model. In the case of micromechanical model the left-hand side reads

$$I_{\mathrm{m}} = \int_0^{\delta_n^{\mathrm{f}}} {d_{\mathrm{m}}}^m \cdot \mathrm{d}\delta_n = \frac{(1-f_{\mathrm{c}})\ (1-f_0)}{(f_{\mathrm{c}}-f_0)} \cdot \frac{\delta_n^{\mathrm{f}}}{g_0^{n+1}} \cdot \int_{f_0}^{f_{\mathrm{c}}} \frac{1}{(1-f)^2} \left[(1-f)^2 + \left(\frac{1}{\sqrt{3}} \ln \frac{1}{f} \right)^2 \right]^{\frac{m+1}{2}} \cdot \mathrm{d}f, \quad \text{(B.5)}$$

where I_{m} is evaluated numerically. Thus, the stress-rupture relation becomes

$$\tilde{I}_k \cdot \frac{\delta_n^{\mathrm{f}}}{\dot{\delta}_0} = \left(\frac{\sigma}{\sigma_0} \right)^m \cdot t_{\mathrm{f}}, \quad \text{(B.6)}$$

where $\tilde{I}_k = I_k / \delta_n^{\mathrm{f}}$.

C Appendix: The damage effects on the physical limits

In this appendix we will develop relations for $\hat{C}_k$-function in the stiff physical limit in the presence of damage, i.e. similar to Eq. (40) in Sect. 4.3. The crack propagation rate is obtained by integration of the relation between the damage parameter and the traction which is derived from the relationship between $\dot{\delta}_n$ and T_n and the damage evolution law as in "Appendix B". Hence, recall the general form of relationship between $\dot{\delta}_n$ and T_n in Eq. (B.1) and following the analysis presented in the main text we can replace (B.1) by

$$\int_{\delta_n^{\mathrm{c}}}^{\delta_n^{\mathrm{f}}} {d_k}^m \cdot \mathrm{d}\delta_n = (n+1)\ \frac{\dot{\delta}_0}{\dot{a}} \left[\frac{C^*}{\dot{\varepsilon}_0\, \sigma_0\, I_n\, r} \right]^{\frac{n}{n+1}} \tilde{\sigma}_\theta\,(n,0)^n\,, \quad \text{(C.1)}$$

As before, we limit consideration to the case of $n = m$ and we assume $\delta_n^{\mathrm{c}} = 0$ for simplicity. The left-hand side is evaluated as in Eqs. (B.3), (B.4) and (B.5). The dimensionless velocity is determined as

$$\overset{\triangledown}{a} = (n+1)\ \frac{\bar{\delta}_n^{\mathrm{f}}\, \bar{r}_{\mathrm{c}}^{\frac{1}{n+1}}}{\phi_0\, \bar{I}_k} \left[\frac{f_n\,(n)}{I_n} \right]^{\frac{n}{n+1}} \tilde{\sigma}_\theta\,(n,0)^n\,, \quad \text{(C.2)}$$

where $\bar{I}_k = I_k / \lambda$. Comparison with Eq. (30) yields the $\hat{C}_k$-function for the case of stiff interface as

$$\hat{C}_k = (n+1)\ \frac{\bar{\delta}_n^{\mathrm{f}}\, \bar{r}_{\mathrm{c}}^{\frac{1}{n+1}}}{\bar{I}_k} \left[\frac{2n}{n+1} \cdot \frac{1}{\phi_0\, I_n} \right]^{\frac{n}{n+1}} \tilde{\sigma}_\theta\,(n,0)^n\,. \quad \text{(C.3)}$$

Comparison with $\hat{C}_k$-function in Eq. (34) and assuming that the size of the damage is similar:

$$\mu_k = \frac{\bar{\delta}_n^{\mathrm{f}}}{\bar{I}_k}. \quad \text{(C.4)}$$

References

Abaqus H (2016) Karlsson and Sorensen. Inc., User's manual version 6.14

Ainsworth RA, Chell GG, Coleman MC, Gooch DJ, Haigh JR, Kimmins ST, Neate GJ et al (1987) Cegb assessment procedure for defects in plant operating in the creep range. Fatigue Fracture Eng Mater Struct 10(2):115–127

Barenblatt GI (1962) The mathematical theory of equilibrium cracks in brittle fracture. Adv Appl Mech 7:55–129

Bassani JL, Hawk DE, Saxena A (1988) Evaluation of the c_t parameter for characterizing creep crack growth rate in the transient regime. In: Nonlinear fracture mechanics: volume I time-dependent fracture. ASTM International, West Conshohocken

Bassani JL, Hawk DE (1990) Influence of damage on crack-tip fields under small-scale-creep conditions. Int J Fract 42(2):157–172

Camacho GT, Ortiz M (1996) Computational modelling of impact damage in brittle materials. Int J Solids Struct 33(20):2899–2938

Cocks ACF, Ashby MF (1981) Creep fracture by void growth. In: Creep in structures. Springer, Berlin, pp 368–387

Cocks ACF, De Voy Julian DJ (1991) A study of creep crack growth in engineering materials. In: Mechanics of creep brittle materials 2. Springer, Berlin, pp 1–13

Cocks ACF, Elmukashfi E, Hu J (2017) To appear

Cocks ACF, Ashby MF (1980) Intergranular fracture during power-law creep under multiaxial stresses. Metal Sci 14(8–9):395–402

Dugdale DS (1960) Yielding of steel sheets containing slits. J Mech Phys Solids 8(2):100–104

Ehlers R, Riedel H (2013) A finite element analysis of creep deformation in a specimen containing macroscopic crack. In: ICF5, Cannes (France) 1981

Elmukashfi E, Kroon M (2014) Numerical analysis of dynamic crack propagation in biaxially strained rubber sheets. Eng Fract Mech 124:1–17

Elmukashfi E, Cocks ACF (2017) To appear

Hillerborg A, Modéer M, Petersson P-E (1976) Analysis of crack formation and crack growth in concrete by means of fracture mechanics and finite elements. Cem Concr Res 6(6):773–781

Hui CY, Riedel H (1981) The asymptotic stress and strain field near the tip of a growing crack under creep conditions. Int J Fract 17(4):409–425

Hui C-Y, Xu D-B, Kramer EJ (1992) A fracture model for a weak interface in a viscoelastic material (small scale yielding analysis). J Appl Phys 72(8):3294–3304

Hutchinson JW (1968) Plastic stress and strain fields at a crack tip. J Mech Phys Solids 16(5):337–342

Kachanov LM (1958) Time of the rupture process under creep conditions. Isv Akad Nauk SSR Otd Tekh Nauk 8:26–31

Knauss WG (1993) Time dependent fracture and cohesive zones. J Eng Mater Technol 115(3):262–267

Landes JD, Begley JA (1976) A fracture mechanics approach to creep crack growth. In: Mechanics of crack growth. ASTM International, West Conshohocken

Lemaitre J, Chaboche J-L (1994) Mechanics of solid materials. University Press, Cambridge

Leung C-P, McDowell DL (1990) Inclusion of primary creep in the estimation of the CT parameter. Int J Fract 46(2):81–104

Miller AG, Ainsworth RA (1989) Consistency of numerical results for power-law hardening materials and the accuracy of the reference stress approximation for J. Eng Fract Mech 32(2):233–247

Needleman A (1987) A continuum model for void nucleation by inclusion debonding. J Appl Mech 54(3):525–531

Needleman A (1990) An analysis of tensile decohesion along an interface. J Mech Phys Solids 38(3):289–324

Nikbin KM, Smith DJ, Webster GA (1983) Influence of creep ductility and state of stress on creep crack growth. Advances in life prediction methods at elevated temperatures, pp 249–258

Nikbin KM, Webster GA, Turner CE (1976) Relevance of non-linear fracture mechanics to creep cracking. In: Cracks and fracture. ASTM International, West Conshohocken

Nikbin KM, Smith DJ, Webster GA (1984) Prediction of creep crack growth from uniaxial creep data. Proc R Soc Lond A Math Phys Eng Sci 396:183–197

Ohji K, Ogura K, Kubo S (1976) Creep crack propagation rate in SUS 304 stainless steel and interpretation in terms of modified J-integral. Trans Jpn Soc Mech Eng 42:350–358

Onck P, van der Giessen E (1998) Growth of an initially sharp crack by grain boundary cavitation. J Mech Phys Solids 47(1):99–139

Ortiz M, Pandolfi A (1999) Finite-deformation irreversible cohesive elements for three-dimensional crack-propagation analysis. Int J Numer Meth Eng 44(9):1267–1282

Ortiz M, Suresh S (1993) Statistical properties of residual stresses and intergranular fracture in ceramic materials. J Appl Mech 60(1):77–84

Rabotnov JN (1969) Creep problems in structural members, vol 7. North-Holland Pub. Co., Amsterdam

Rahul-Kumar P, Jagota A, Bennison SJ, Saigal S, Muralidhar S (1999) Polymer interfacial fracture simulations using cohesive elements. Acta Mater 47(15):4161–4169

Rice JR (1978) Mechanics of quasi-static crack growth. Technical report, Division of Engineering, Brown University, Providence

Rice JR, Rosengren GF (1968) Plane strain deformation near a crack tip in a power-law hardening material. J Mech Phys Solids 16(1):1–12

Rice JR, Wang J-S (1989) Embrittlement of interfaces by solute segregation. Mater Sci Eng A 107:23–40

Riedel H (1981) Creep deformation at crack tips in elastic-viscoplastic solids. J Mech Phys Solids 29(1):35–49

Riedel H (1987) Fracture at high temperatures. Springer, Berlin

Riedel H, Rice JR (1980) Tensile cracks in creeping solids. In: Fracture mechanics. ASTM International, West Conshohocken

Saxena A (1986) Creep crack growth under non-steady-state conditions. In: Fracture mechanics: seventeenth volume. ASTM International, West Conshohocken

Taira S, Ohtani R, Kitamura T (1979) Application of J-integral to high-temperature crack propagation: part-i creep crack propagation. J Eng Mater Technol 101(2):154–161

Thouless MD, Hsueh CH, Evans AG (1983) A damage model of creep crack growth in polycrystals. Acta Metall 31(10):1675–1687

Tvergaard V (1984) On the creep constrained diffusive cavitation of grain boundary facets. J Mech Phys Solids 32(5):373–393

Tvergaard V (1990) Effect of fibre debonding in a whisker-reinforced metal. Mater Sci Eng A 125(2):203–213

Van Der Giessen E, Tvergaard V (1994) Development of final creep failure in polycrystalline aggregates. Acta Metall Mater 42(3):959–973

Wang H, Lu W, Barber JR, Thouless MD (2016) The roles of cohesive strength and toughness for crack growth in viscoelastic and creeping materials. Eng Fract Mech 160:226–237

Wen J-F, Shan-Tung T (2014) A multiaxial creep-damage model for creep crack growth considering cavity growth and microcrack interaction. Eng Fract Mech 123:197–210

Willam K, Stankowski T, Runesson K, Sture S (1989) Simulation issues of distributed and localized failure computations. In: Mazars J, Bazant ZP (eds) Cracking and damage. Elsevier, New York, pp 363–378

Xu X-P, Needleman A (1993) Void nucleation by inclusion debonding in a crystal matrix. Modell Simul Mater Sci Eng 1(2):111

Yalcinkaya T, Cocks A (2015) Physics based formulation of a cohesive zone model for ductile fracture. In: Key engineering materials, vol 651. Trans Tech Publ, Zurich, pp 993–999

Yatomi M, Nikbin KM (2014) Numerical prediction of creep crack growth in different geometries using simplified multiaxial void growth model. Mater High Temp 31(2):141–147

Yu C-H, Huang C-W, Chen C-S, Gao Y, Hsueh C-H (2012) Effects of grain boundary heterogeneities on creep fracture studied by rate-dependent cohesive model. Eng Fract Mech 93:48–64